Materials and Design 192 (2020) 108718

Contents lists available at ScienceDirect

Materials and Design

journal homepage: www.elsevier.com/locate/matdes

Investigations on the mechanism of microweld changes during ultrasonic wire bonding by molecular dynamics simulation

Yangyang Long [a,*], Bo He [b], Weizhe Cui [a], Yuhang Ji [a], Xiaoying Zhuang [b], Jens Twiefel [a]

[a] Institute of Dynamics and Vibration Research, Leibniz Universität Hannover, Appelstr. 11, 30167 Hannover, Germany
[b] Institute of Continuum Mechanics, Leibniz Universität Hannover, Appelstr. 11, 30167 Hannover, Germany

HIGHLIGHTS

- The mechanism of microweld formation and breakage was studied for the first time.
- The mechanism of microweld changes under different configurations was investigated.
- The significant impact factors on microweld changes were analyzed.
- A large deformation and a middle-level amplitude are helpful for microweld growth.

GRAPHICAL ABSTRACT

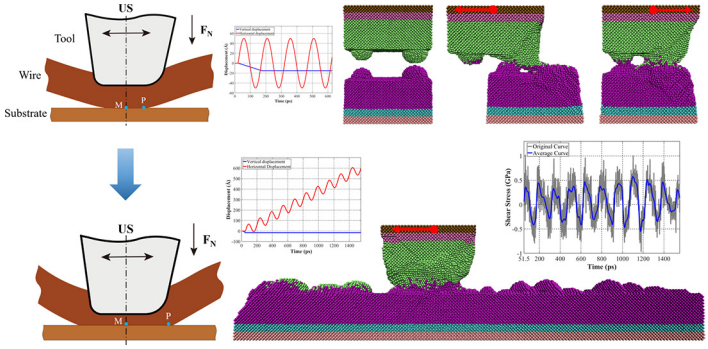

ARTICLE INFO

Article history:
Received 10 February 2020
Received in revised form 24 March 2020
Accepted 3 April 2020
Available online 5 April 2020

Keywords:
Microweld formation & breakage
Bonding mechanism
Molecular dynamics simulation
Ultrasonic wire bonding

ABSTRACT

Despite the wide and long-term applications of ultrasonic (US) wire bonding and other US metal joining technologies, the mechanism of microweld changes during the bonding process, including formation, deformation and breakage, is rarely known as it is very difficult to be investigated by experiments. In this work, this mechanism under different surface topographies and displacement patterns is studied by molecular dynamics simulation. It is found that microwelds can be formed or broken instantly. Due to the relative motion between the local wire part and the local substrate part, microwelds can be largely deformed or even broken. The impacts of material, surface topography, approaching distance and vibration amplitude on the microweld changes are investigated via the quantification of the shear stress and the equivalent bonded area. It is shown that these four factors significantly influence the final connection and the interface structure. The analysis of the scale influence on the microweld changes shows that the simulation results at a small-scale are able to represent those at a large-scale which is close to the range of the commonly used surface roughness. This deeper understanding on the microweld changes leads to a better control strategy and an enhancement of the bonding process.

1. Introduction

Ultrasonic (US) wire bonding, which applies a normal force and US vibration to join wire and substrate, is a widely used interconnection technique in electronic packaging industry since its invention in the 1960s [1]. Nowadays, about one million bonds per second in integrated

* Corresponding author.
E-mail address: long@ids.uni-hannover.de (Y. Long).

https://doi.org/10.1016/j.matdes.2020.108718

circuits (ICs), transistors, power devices and other special applications are made globally by this technique [2]. Despite its wide and long-term applications, the underlying mechanisms are still not well understood, due to the short processing time (tens of milliseconds), the high vibration frequency (60–150 kHz), the enclosed interface and the highly dynamic changes. Among these mechanisms, the knowledge on the changes of microwelds at the wire/substrate interface during the bonding process, including the formation, deformation and breakage of microwelds, is particularly limited. Since bonds are constituted by numerous microwelds, the bonding quality is determined by the microweld changes, specifically by the competition between the formation, deformation and breakage. The same goes for the other US metal joining processes, including US wire welding, US metal welding and US metal consolidation, in which the microwelds determine the joining quality. The lack of knowledge in this aspect prevents further enhancement of these joining processes.

According to [2,3], the bonding process can be divided into four phases namely: pre-deformation and activation of vibration, friction, US softening and interdiffusion. The last three phases overlap with each other. The pre-deformation of the wire caused by the normal force loading creates an elliptic contact between the wire and the substrate and cracks of the oxide layer [4]. After US activation, the wire starts to slide on the substrate and relative motions between the wire and the substrate are generated [5,6]. During this friction phase, the oxides within the contact interface are detached from the metal surface and transported to the peripheral or outside contact region [4,7]. The US vibration also brings a softening effect which causes the bulk deformation of the wire and the deformation of the surface asperities [8–10]. This bulk deformation also causes a relative motion between wire and substrate. The deformation of asperities brings more local areas closer. As local oxides are removed and the pure metal surfaces in this location come into contact, a microweld is formed. Evidence has been demonstrated in previous studies in which a distance of 3 nm during the approaching of local wire and substrate surfaces has been captured by a high resolution transmission electron microscope [11]. This suggests that the formation of microwelds takes place at an atomic level. As the process continues, more microwelds are formed and the total microweld area increases.

Due to the relative motion between wire and substrate, microweld formation is also accompanied by the deformation and breakage of microwelds. As mentioned before, both the vibration and the bulk deformation of the wire cause the relative motion. Therefore, different locations of the wire/substrate interface have different relative motion patterns. This difference is illustrated in Fig. 1. Fig. 1(a) and (b) shows the bonding status in the beginning and ending stage, respectively. The substrate can be considered to be fixed since its vibration amplitude is negligible. The equilibrium position of the local wire part in the middle of the contact stays in its original position. The equilibrium position of the local wire part in the peripheral contact region moves outwards. Thus the "M" part of the wire conducts a sinusoid movement as in Fig. 1 (c) while the "P" part of the wire runs in the pattern as shown in Fig. 1 (d). If the dimension of the microweld at "M" position is smaller than the vibration amplitude, it is supposed to be broken. When the absolute horizontal movement of the "P" wire part exceeds the microweld dimension, a large deformation or even breakage of the local microwelds is also expected. However, the deformation and breakage of microwelds have been rarely mentioned and studied in the literature [2,12]. Most works only refer to microweld formation.

In the past, there are generally four methods utilized to analyze microwelds. The most straightforward one is via shear tests [13,14]. When the ultimate shear stresses of the bonding materials are known, the total microweld area can be calculated by the ratio of the shear force over the ultimate shear stress [7]. However, shear tests are destructive and can therefore only be performed once for each bond. This renders the changes of microwelds during the bonding process non-detectable. The second most commonly used method is optical observation with a microscope, mostly a scanning electron microscope (SEM) [15–17]. When the wire or the substrate material is removed, e.g., through chemical etching or mechanical removal, the exposed interface can be directly observed. After thousands of vibration (scrub)

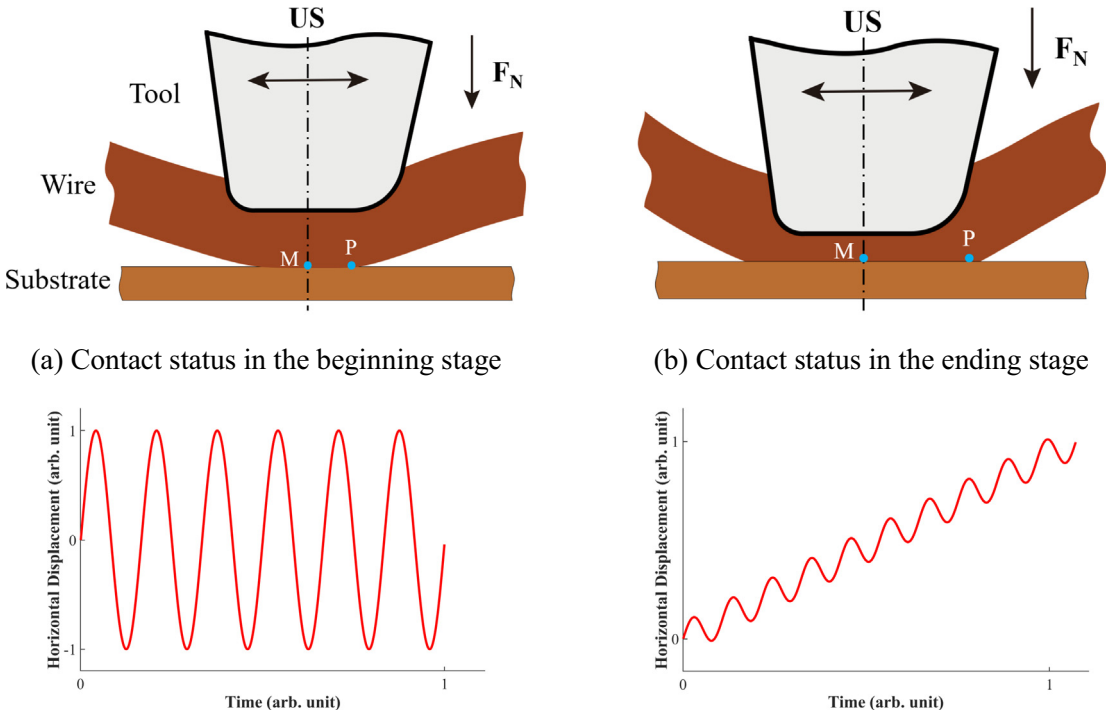

Fig. 1. Illustration of different horizontal displacement patterns of the wire parts at different locations of the wire/substrate interface (M: middle; P: peripheral).

cycles, the surface topography is significantly changed. This makes non-welded areas, where microwelds have been broken due to vibration during the bonding process, indistinguishable from microweld areas where microwelds are broken due to the removal of wire or substrate after the bonding process. The surface topographies of these areas are similar to each other. In other words, the observation of the exposed interface can only reveal the information of topography changes but not the existence of microwelds. When the wire is not completely removed and some residues are left, the direct observation of the underlying microwelds is hindered [2,15]. Therefore, this method is unfavorable in analyzing the changes of microwelds. The third method is the measurement of contact resistance, in which the start of microweld formation as well as the growth of microweld area during the bonding process are detected [14,18]. The sudden drop of the contact resistance during the first couple of milliseconds indicates the formation of the first microweld while the slow decrease of the contact resistance exhibits the growth of the microweld area. This method, however, only shows the average formation of microwelds while the deformation and breakage of microwelds are not detectable. The last method is via the analysis of vibration [12]. Based on the measurement of the vibration amplitude of the tool tip, the bonding process was divided into different stages including sliding, adhesion, balance between adhesion and separation, and separation. In this study, the separation (or breakage) of microwelds was first proposed. However, it is not often that the tool tip vibration amplitude has such a profile. It becomes very complex when all stages contain multi-frequencies. Furthermore, this method cannot explain local changes of microwelds. The advantages and disadvantages of these methods are summarized in Table 1.

From the past research work, it can be seen that it is nearly impossible to investigate the local changes of microwelds by experiments. In this case, simulation becomes the only possible approach. Since the changes of microwelds take place at an atomic level, molecular dynamics (MD) simulation is used in this work to investigate the local changes of microwelds. In recent years, MD simulation has been extensively used to study various manufacturing processes. Substantial MD simulations were made on precision machining and polishing of silicon as well as other hard and brittle materials, which helped the understanding of the material removal, brittle-to-ductile translation, subsurface damage, residual stress, and tool wear mechanisms [19–24]. US vibration has been added in MD models to study the surface quality improvement, impact effect and material removal [24–27]. Additive manufacturing including sintering and 3D printing was also investigated by MD simulations to analyze the thermodynamic process [28–30]. Specifically, MD models have been established for welding processes to study the thermomechanical properties and mass transfer behavior [31–33]. For US joining processes, the diffusion behavior was studied and the results showed that US vibration has a significant impact on enhancing the diffusion during the joining processes [34–36]. In these welding studies, only the joining of the two welding partners was considered. The dynamic behavior of microwelds associated with US joining processes, especially the deformation and breakage, has not been mentioned yet. This forms the main contribution of this work.

Table 1
Pros and cons of different experimental methods for microweld measurements.

Methods	Pros	Cons
Shear test	Fast; quantitative	Destructive; non-detectable of microweld breakage
Interface observation	Intuitive	Destructive; indistinguishable between formation and breakage
Contact resistance	Real-time; non-destructive; quantitative	Low-accuracy in the later stage; non-detectable of microweld breakage
Vibration analysis	Non-destructive	Low repeatability; qualitative; non-detectable of local changes

It shall be noted that the small-scale (ps and Å level) simulation in this work can represent the microweld changes at the large-scale (μs and μm level) to a large extent despite the big differences. First, even though the amplitude of actual ultrasonic bonding process is at micron level, the formation and breakage of microwelds occur at angstrom level. The nature of a microweld is the direct contact of the atoms from the local surfaces of the bonding partners. Contact is defined as the atoms from one bonding partner reaches the lowest interatomic potential energy position of the atoms from the other bonding partner. Second, the formation and breakage of a microweld or metallic bonds take place in a short time (<μs). They have no direct relation with the vibration period. Third, the simulation at ps level confirmed that an impact effect will not occur during actual vibration at μs level. That the simulation period is much smaller than the actual vibration period means that the velocity in the simulation is much higher than that in actual processes. Since obvious impact effect of the moving part on the static part was not observed in our preliminary study, it will not occur when the speed is greatly decreased. From this point of view, the simulation results at ps level are transferrable to those at μs level. Fourth, successful bonds have been made on a smooth surface with a roughness at nm level which is similar to the dimensions of the MD model [4,7]. Lastly, the volume of the MD model in this work was enlarged by 27 times to further confirm the representability of the small scale model. Results and discussion can be found in Section 4.5.

In the following sections, the MD simulation and the model establishment are first briefly described. Details on the microwelds changes under different conditions are then provided. The shear stress and the equivalent bonded area are quantified. Finally, the scaling problem is discussed.

2. Molecular dynamics modeling

2.1. Geometries of MD models

As described above, microwelds are formed at the tips of asperities during the approaching of the local wire and local substrate surfaces. According to [7,9,37], the bonding strength does not decrease when the surface roughness is smaller than 10 nm. In this work, a local part of the wire and the corresponding local part of the substrate were built up to model the formation, deformation and breakage of microwelds. The basic geometry of the model with surface topography 1 (ST1) is shown in Fig. 2. Two different joining pairs, Al-Al and Cu-Cu, were used, as shown in (a) and (b) respectively.

There are two parts in the model: the local wire (upper part) and the local substrate (lower part). Each part consists of three different layers: a sliding layer, a thermo-layer and a Newton layer. The sliding layers were used to provide the desired displacements. For the substrate part, this layer was fixed throughout the simulation duration. The displacements imposed on the wire part will be described in the following subsection. The thermo-layers were used to control the temperature. The initial temperature of the thermo-layers was set at 300 K. During the following process, the temperature of these layers will be rescaled to 300 K once it was out of the range 290–310 K (as validated by the results, the temperature of the thermo-layer was well kept in the range of 290–310 K throughout the whole process). In this way, the influence of temperature was minimized and the influence of vibration can be emphasized. The Newton layers served as the reaction layers where microwelds were formed, deformed and broken. To simulate asperities, two half-spheres were created in the Newton layers of both the wire and the substrate part. The distance between the two asperities is intended to be larger so that the change of individual asperities as well as their interactions can be better studied. The larger asperities have a radius of 19 Å and the radius of the smaller ones is 15 Å. For Al-Al bonding, there are in total 40,450 atoms. As copper atoms (r: 128 pm) are smaller than aluminum atoms (r: 143 pm), the Cu-Cu model contains 55,230 atoms.

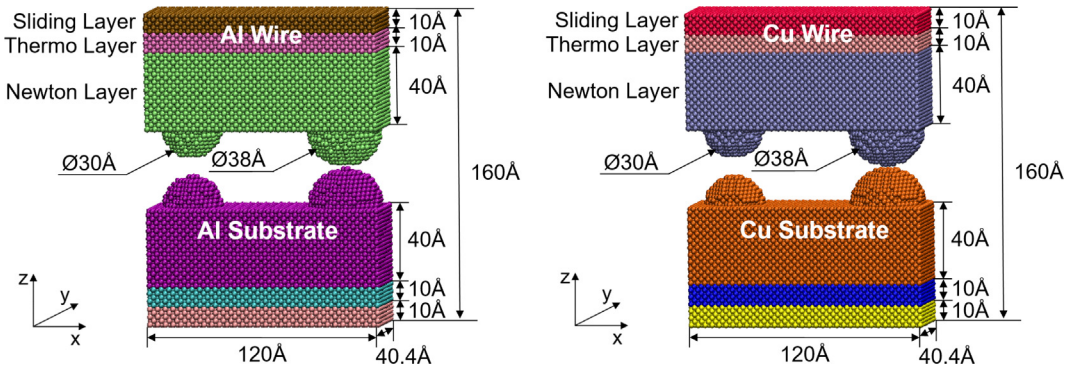

(a) Al-Al (b) Cu-Cu

Fig. 2. Geometries of the ST1 molecular dynamics models.

The surface topography and the dimensions of the model will be varied to investigate their influence on the microweld changes. Details of the alternative geometries will be provided in the corresponding parts of Section 4. The simulations were performed in Large-scale Atomic/Molecular Massively Parallel Simulator (LAMMPS) provided by Sandia National Research Lab [38] and the results were visualized in Visual Molecular Dynamics (VMD) provided by Theoretical Biophysics Group of University of Illinois [39].

2.2. Force field

After the building-up of the geometries, the force field that defines the pairwise interactions among atoms, must be selected for the MD simulations. In this work, the most frequently used and accurate method - embedded-atom method (EAM) was applied. It was developed by Daw and Baskes [40,41]. The total potential energy E that a single atom i receives is calculated as:

$$E_i = \sum_i F(\rho_i) + \frac{1}{2}\sum_{i \neq j} \varphi(R_{ij}) \tag{1}$$

$$\rho_i = \sum_j d(R_{ij}) \tag{2}$$

where F is the embedding energy expressed as a function of ρ_i, ρ_i is the electron density at atom i; R_{ij} is the distance between atoms i and j; φ is the short-range electrostatic pair potential; and d is the electron density function at atom i due to atom j.

The specific EAM parameters for face-centered cubic (fcc) Al and fcc Cu were obtained from Jacobsen et al. [42] and Foiles et al. [43], respectively.

2.3. Boundary conditions

In Section 2.1, it has been stated that the sliding layer of the substrate was fixed the thermo-layer was kept in the range of 290–310 K throughout the simulation duration. In this section, the displacements imposed on the sliding layer of the wire part are described. In general, three different displacement patterns (DP) were applied in this work:

DP1: the wire part first moved down to touch the substrate part and then moved horizontally. The moving route of DP1 is shown in Fig. 3 (a). After a 20 ps relaxation, the wire part moved down (−z) for 1.5 nm at a velocity of 0.4 Å/ps; with no further vertical movement, the wire part then moved rightwards (+x) for 17 nm at a velocity of 0.5 Å/ps; the wire part then sequentially moved to the left and to the right for 34 nm at a velocity of 0.5 Å/ps. This DP is not the DP during wire bonding, but serves as a guide to study the individual effect of the vertical and horizontal movement on the formation, deformation and breakage of microwelds. The solely vertical movement in the beginning stage allows the formation of microwelds, which directly corresponds to the approaching of wire and substrate surfaces as mentioned above. The horizontal displacement which is larger than the x-dimension of the model, confirmed the occurrence of microweld breakage.

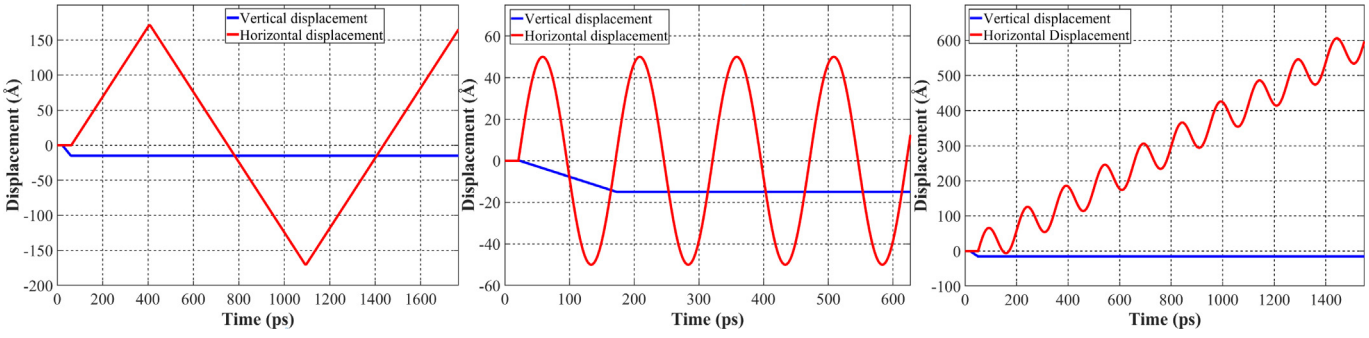

(a) DP1 (b) DP2 (c) DP3

Fig. 3. Displacements imposed on the wire part.

DP2: while the wire part was moving down, it also moved horizontally and did not stop when the vertical movement finished. The moving route of DP2 is shown in Fig. 3(b). After a 20 ps relaxation, the wire part moved vertically and horizontally at the same time. The downwards movement lasted for 150 ps with a velocity of 0.1 Å/ps. The horizontal movement was defined as a sinusoid movement:

$$x = 50\ \sin\left(\frac{2\pi}{150}t\right)\ \text{Å}\ (20\ \text{ps} \le t \le 620\ \text{ps}) \tag{3}$$

Except in dimension, this DP is similar to that in the central region of the bonding interface, where the sliding distance is ignorable. The vibration amplitude, which is smaller than the x-dimension of the model, is used to analyze the changes of the microwelds and the surface topographies, when the size of microwelds is equivalent to the vibration amplitude.

DP3: After a 20 ps relaxation, the wire part first moved down to touch the substrate part. The wire then horizontally slid on the substrate with additional vibration simultaneously. As shown in Fig. 3 (c), the horizontal moving route of DP3 is defined as:

$$x = 0.4\,t + 50\ \sin\left(\frac{2\pi}{150}t\right)\ \text{Å}\ (50\ \text{ps} \le t \le 1550\ \text{ps}) \tag{4}$$

In addition to a constant velocity of 0.4 Å/ps, a sinusoidal vibration with a displacement amplitude of 50 Å was superimposed on the wire part for the horizontal (x-axis) movement. Except in dimension, this DP is similar to that in the peripheral region of the contact where both sliding and vibration occur. It is mainly used to study the change of the surface topographies under repeated microweld formation and breakage.

For different STs and dimensions, the DPs were finely adjusted while the main characteristics of the DPs stayed the same. Details will be provided in corresponding parts of Section 4.

2.4. Calculation of shear stress and bonded area

As microwelds are formed, deformed and broken, the stresses also change. The virial stress is calculated as:

$$\sigma^{\alpha\beta} = \frac{1}{V}\sum_i \left[\frac{1}{2}\sum_{ij} f_{ij}^{\alpha} R_{ij}^{\beta} - m_i v_i^{\alpha} v_i^{\beta}\right] \tag{5}$$

where V is the calculated volume (in this work, it is the 10 Å thick layer of the substrate Newton layer); f_{ij} is the interaction force between atom i and j; m is the mass of the atom i; and v_i^{α} is the velocity of atom i in α direction. As the tangential stress is the most related stress with the bonding strength, it is the focus of this work. Even though the real values are not reflected due to the dimension and defect issues, it can still indicate the influence of vibration on the changes of microwelds.

Since the surface topography greatly changed under the different movements of the wire part, it is very difficult to directly track the bonded area (microweld area). In this work, the microweld area was estimated by an equivalent area A_e which was defined as:

$$A_e = \frac{|\tau|}{\tau_{\max}} A_S \tag{6}$$

where $\tau_{\max}$ is the ultimate shear stress of a nano-cube and A_S is the x-y area of the wire or substrate part. $\tau_{\max}$ is obtained by the simulation of the shear test of the nano-cube (a single crystal). The nano-cubes are shown in Fig. 4, where the green cube and silver cube represent Al and Cu, respectively. The corresponding stress-strain curves are also shown in Fig. 4. It can be seen that from zero strain to 0.186 (0.174 for Cu), no defect existed and the nano-cube was only elastically deformed. Along with the increase of the strain, the shear stress linearly increased. After the ultimate point, the transition from elastic deformation to plastic deformation occurred. The defects of the crystal caused a sudden drop of the shear stress. At 0.25 strain, most of the lattice structure within the cube was destroyed. These results are in agreement with the literature [44]. It can be seen that the equivalent area A_e is not the real bonded area. Nevertheless, the equivalent area can still indicate the changes of the bonded area and the changes of the surface topographies. Therefore, it will be used and discussed to obtain a quantitative understanding of these changes. According to Eq. (6), it can also be seen that the frequency of the equivalent area will be twice of that of the shear stress when the wire part oscillates around its equilibrium position.

3. Results and discussion on ST1

3.1. Microweld changes under DP1

As described in Introduction, the formation of a microweld is achieved by a direct contact of local wire and substrate surfaces. The direct approaching of the two surfaces is shown in Fig. 5. Since the asperities are half spheres, the potential energies of the tip atoms were stable and the symmetric geometries were not significantly disturbed during approaching, as shown in Fig. 5(a)–(b). This is in accordance to the transmission electron microscope observation [11]. Naturally, the first microweld was formed at the tall asperities when the tip atoms contacted each other. As the vertical motion of the wire part continued, the microweld grew to a larger area as in Fig. 5(c). The same formation process took place for the smaller asperities in Fig. 5(d)–(e) when the larger asperities further deformed. This indicates the importance of

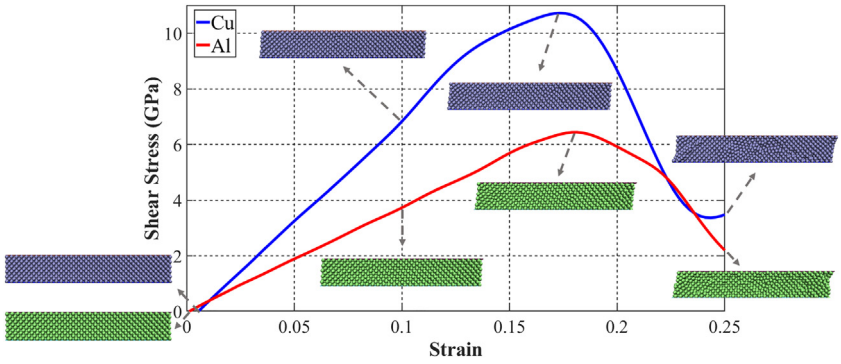

Fig. 4. Stress-strain curves of Al and Cu derived by MD simulation of shear tests.

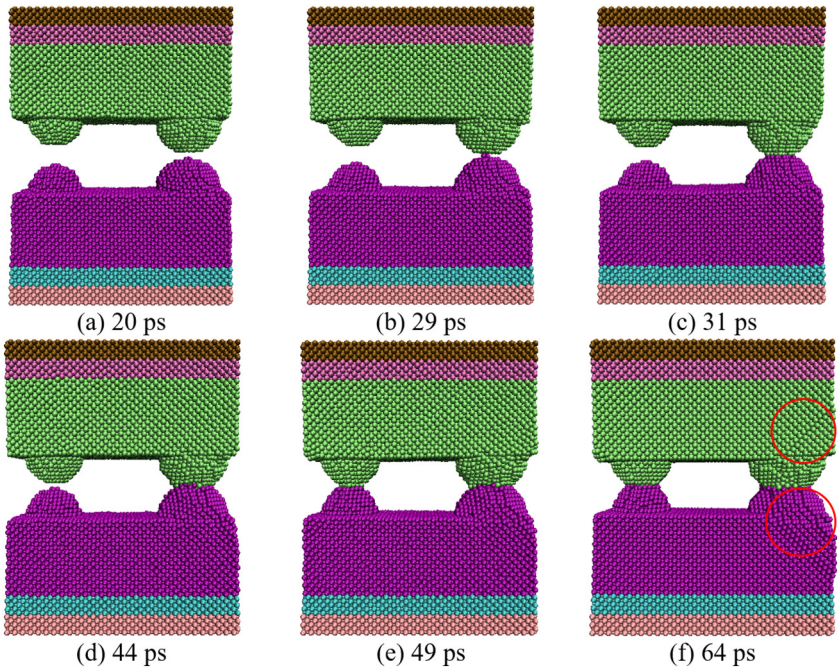

Fig. 5. Formation of microwelds with ST1-DP1 Al-Al.

the asperity deformation on bond formation [45]. In actual bonding process, a larger real contact area is obtained when tall asperities are greatly deformed. When the gap between the wire and the substrate finally decreased to 25 Å, the normal stress at the larger microweld became too large. This large stress caused dislocations in the adjacent region, as marked in Fig. 5(f).

After the vertical motion ended, the wire part started to move rightwards (+x). As shown in Fig. 6(a), both microwelds were deformed due to the horizontal movement. As the displacement increased, the microwelds became more deformed and the smaller microweld was even broken. This process is shown in Fig. 6(b)–(c). In the meantime, the larger microweld stayed connected. As the motion continued, the larger microweld was also broken while the smaller asperity of the wire part got closer to the larger asperity of the substrate part, as shown in Fig. 6(d). A new microweld was then formed by the smaller asperity of the wire part and the larger asperity of the substrate part (see Fig. 6(e)). With further movements, this new microweld was largely deformed as in Fig. 6(f) and finally broken as in Fig. 6(g). The large stresses during the deformation of these microwelds also caused dislocations as depicted in the images.

When the wire part moved to the left side (−x), the smaller asperity of the wire part and the larger asperity of the substrate part were reconnected as shown in Fig. 7(a). This indicates that new microwelds can be formed with the same asperities or at the same locations where old microwelds had been broken. The larger asperity of the wire then touched the larger asperity of the substrate again and another microweld was formed, as shown in Fig. 7(b). In the meantime, the microweld formed by the smaller asperity of the wire part and the larger asperity of the substrate part was substantially deformed. Large amounts of atoms moved along with the deformation of the microweld to fill the valley between the asperities of the substrate. With another few picoseconds as in Fig. 7(c), the two asperities of the substrate part merged together. The surface topography of the substrate part was greatly changed. As the leftwards movement continued, the smaller asperity of the wire part was disconnected with the substrate part as in Fig. 7(d) and then the microweld formed by the larger asperity of the wire part was also broken. As the wire part moved away from the substrate part, a flattened surface from the front view was generated.

When the wire moved to the right side for the second time, all four asperities merged into one microweld, as shown in Fig. 7(e). This led to

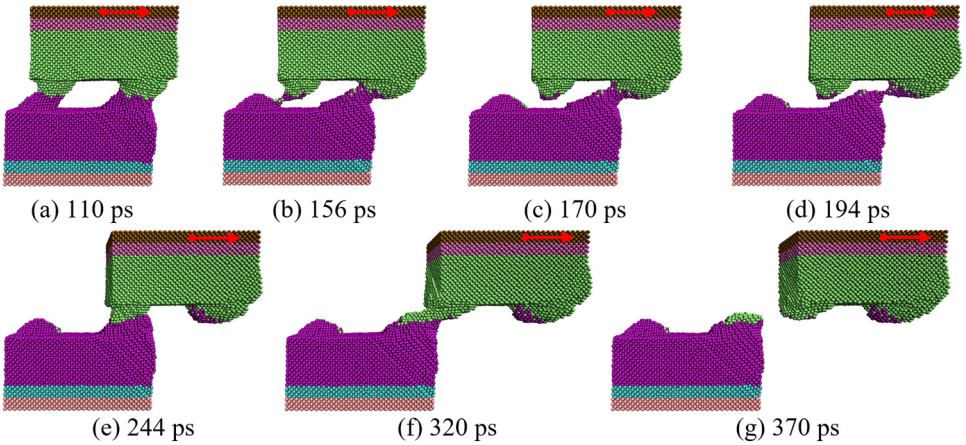

Fig. 6. Breakage and re-formation of microwelds with ST1-DP1 Al-Al during the 1st rightwards movement.

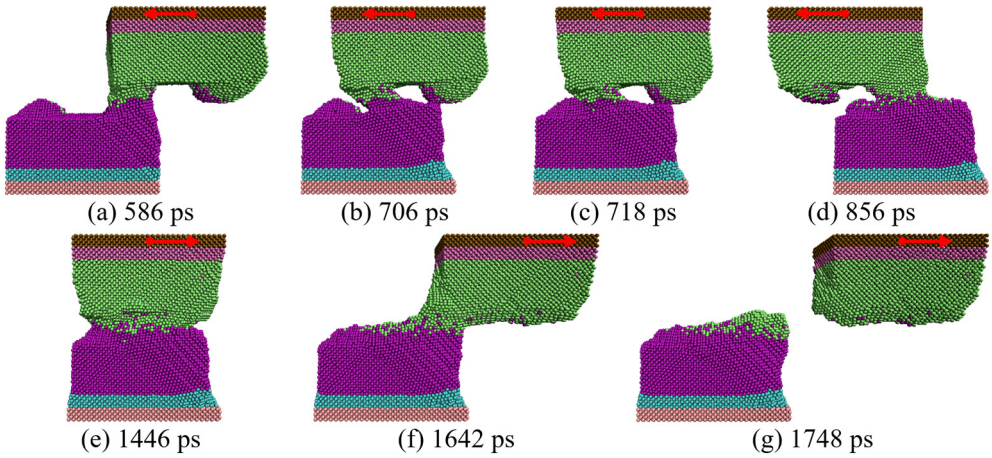

Fig. 7. Breakage and re-formation of microwelds with ST1-DP1 Al-Al during the leftwards movement (a–d) and the 2nd rightwards movement (e–g).

a larger bonded area. As the horizontal displacement continued, the microweld area decreased until the two surfaces were separated, which are shown in Fig. 7(f)–(g). During the separation, many atoms from the wire part were left on the substrate part. For actual bonding, this makes the experimental analysis of microwelds much more difficult.

The whole process described in this section revealed four facts. First, an asperity that comes from a broken microweld can form a new microweld even at its original position, as long as it is able to get into contact with the surface atoms of the bonding partner. Second, the shape of the asperities or the surface topographies can be greatly changed under the repeated horizontal movement, especially for large asperities. Third, large amounts of dislocations are formed during the repeated formation, deformation and breakage of microwelds. Finally, the formation and breakage of microwelds are at the atomic level and occur within an extremely short time.

Fig. 8(a) shows the change of the shear stress during the above-described process. When the rightwards movement started, the shear stress soon increased. After reaching its first peak value around 94 ps, the shear stress decreased as both the two microwelds were largely deformed and the total microweld area decreased. When both microwelds were broken, the stress decreased to zero. The formation of the new microweld (Fig. 6(e)) resulted into the second peak of the stress. As this microweld was broken, no shear stress existed. During the leftwards movement, repeated microweld formation and breakage occurred and caused the fluctuation of the stress. The peak value of the shear stress, however, stayed similar around 0.2 GPa. The peak shear stress significantly increased during the second rightwards movement when the whole surfaces joined together. The change of the equivalent bonded area in Fig. 8(b) is consistent with the change of the shear stress. In general, the joining of the two surfaces was greatly enhanced via the horizontal movement. The maximal microweld area increased from 228 Å^2 in the beginning to 308 Å^2 in the end.

3.2. Microweld changes under DP2

Under DP2, the wire part moved simultaneously in both the vertical and horizontal directions during the first vibration cycle. Since the gap between the two larger asperities was small, the two tips soon approached each other and a small microweld was formed as in Fig. 9(a). Due to the horizontal movement, this microweld was immediately broken, as shown in Fig. 9(b). When the wire part turned back, a larger area of the larger asperities came into contact due to the further vertical movement. The newly formed microweld is larger than the old one, as shown in Fig. 9(c). As the wire part moved further to the left, this microweld became largely deformed but was still connected, as shown in Fig. 9(d). This indicates that the larger microweld was already strong enough to withstand the tangential force brought by the vibration. At the end of the first vibration cycle, the smaller asperity of the wire part touched the smaller asperity of the substrate part on the side and formed another microweld, as shown in Fig. 9(e). During the second vibration cycle, the smaller microweld was broken, re-formed, and deformed. These changes continued as long as this microweld was not strong enough to withstand the tangential stress. Simultaneously, the larger microweld was greatly deformed. Due to this deformation, the larger asperity of the substrate part touched both asperities of the wire part and formed two microwelds in the third vibration cycle, as in Fig. 9(f). In the fourth vibration cycle, both asperities of the wire part contacted the larger asperity of the substrate part, as shown in Fig. 9(g). In addition, the wire part was seriously distorted due to the large tangential stress. The final surface topography

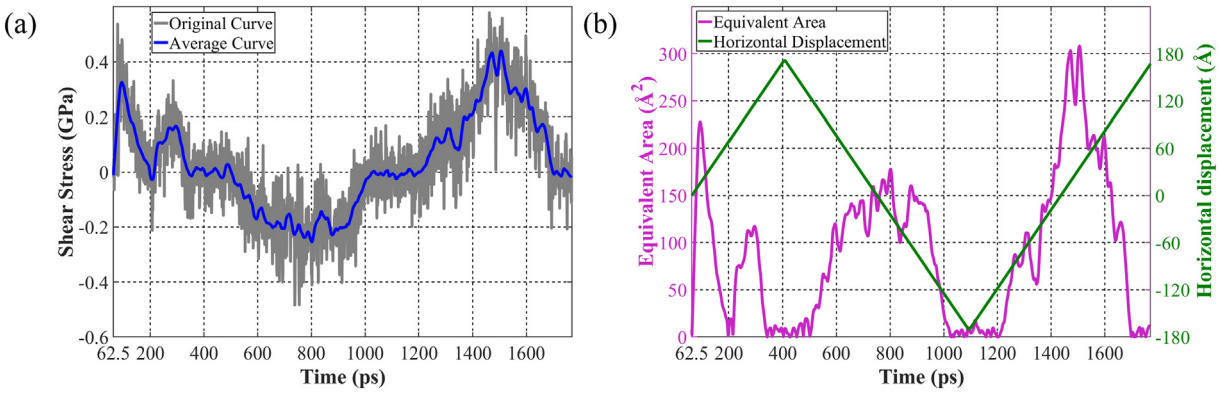

Fig. 8. (a) Shear stress (b) equivalent bonded area with ST1-DP1 Al-Al.

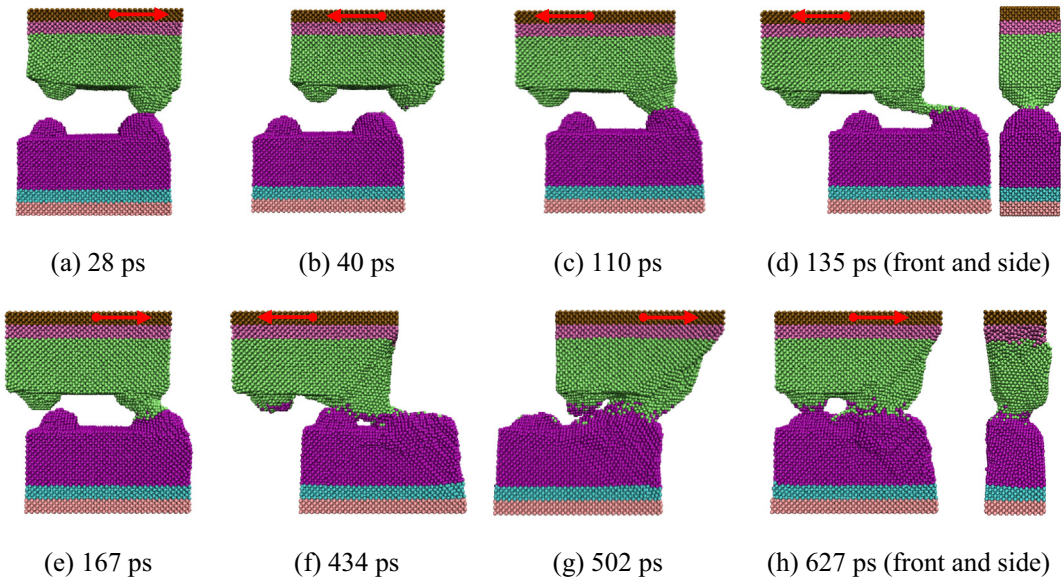

Fig. 9. Breakage and re-formation of microwelds with ST1-DP2 Al-Al.

after four vibration cycles is shown in Fig. 9(h). Compared to the original surface topography, the asperities from both surfaces were flattened.

Fig. 10 shows that the microweld formed in the very beginning did not cause too much stress due to its small size. The first evident peak in both (a) and (b) emerged when the microweld in Fig. 9(c) was formed. As the smaller asperities formed an additional microweld and the larger microweld grew, the equivalent bonded area significantly increased. After the vertical movement finished, the microweld area greatly increased to 207 Å^2. In the rest process, the horizontal vibration gradually increased the bonded area 232 Å^2. From this aspect, the vibration enhances the growth of the microweld area while the vertical movement plays a more significant role.

3.3. Microweld changes under DP3

Under DP3, the wire part first moved downwards in order to touch the substrate. The initially formed microwelds are shown in Fig. 11(a). During the first vibration cycle, the two microwelds were not broken. Furthermore, the total microweld area increased due to the vibration and the constant rightwards movement. This led to the large shear stress during the second vibration cycle and caused the deformation of the substrate Newton layer, as marked in Fig. 11(b). The increase of the shear stress and the equivalent area is reflected in Fig. 12(a) and (b), respectively. From Fig. 11(b), it can also be seen that the horizontal movement greatly changed the surface topography of the wire part which became flat from the front view. During the 4th vibration cycle, the whole wire surface came into contact with the substrate surface (from the front view), as marked in Fig. 11(c). The shear stress and the equivalent area in Fig. 12 also show larger peak values around 600 ps. When the wire part left this area, the substrate surface became flat, as shown in Fig. 11(d).

In the rest process, similar formation, deformation and breakage of microwelds took place. Images from the 6th and 7th cycle are shown in Fig. 11(e) and (f), respectively. During this period, the surface of the marked area in Fig. 11(e) was flattened. At the moment of Fig. 11(f), the highest shear stress (0.577 GPa) and the largest bonded area (404 Å^2) are shown in Fig. 12. In Fig. 11(g), the leftwards movement deformed the microweld which was still well connected. With two further cycles, the wire part left the substrate part and the substrate surface became smoother, as shown in Fig. 11(h). Compared to the original surface in Fig. 11(a), the surface topographies of both the wire and the substrate were greatly changed. This indicates that the constant horizontal movement played a significant role in changing the surface topographies.

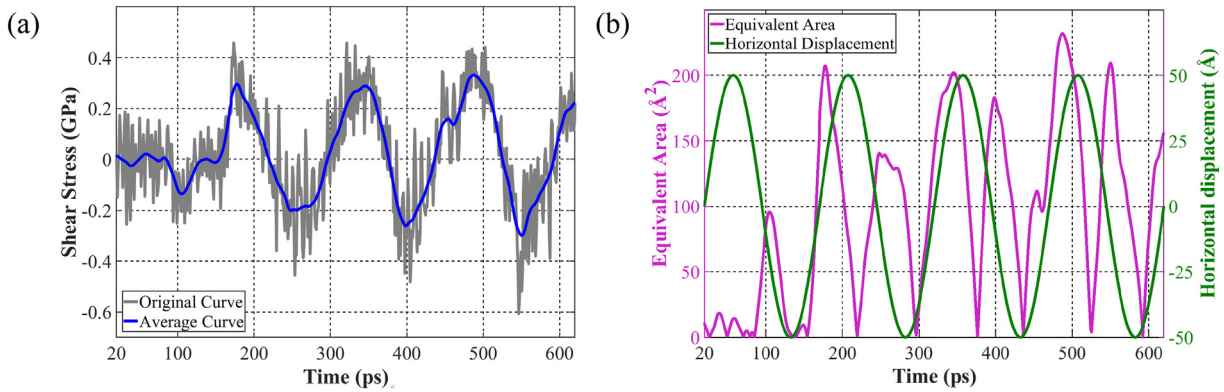

Fig. 10. (a) Shear stress (b) equivalent bonded area with ST1-DP2 Al-Al.

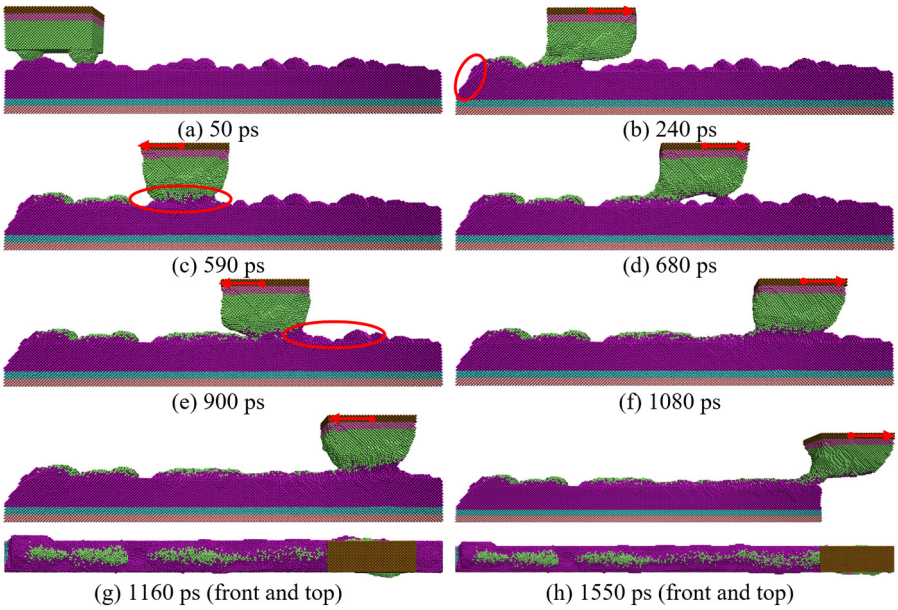

Fig. 11. Breakage and re-formation of microwelds under ST1-DP3 Al-Al.

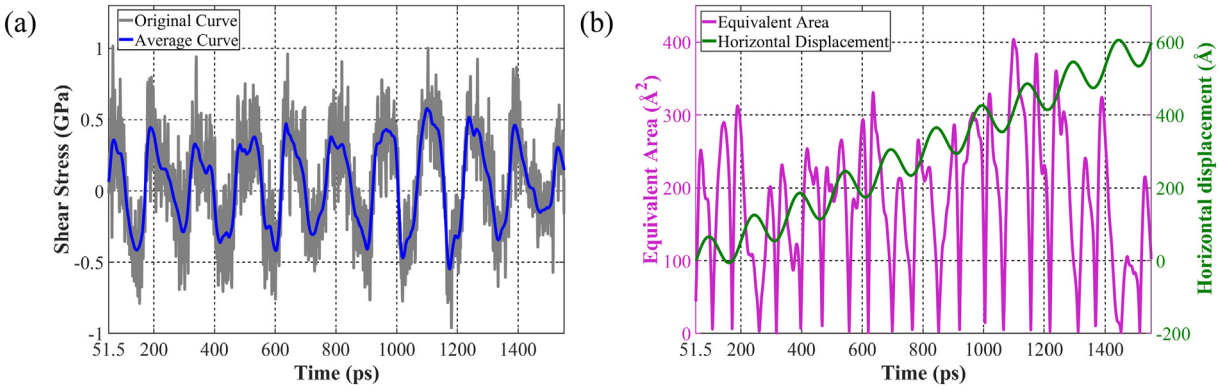

Fig. 12. (a) Shear stress (b) equivalent bonded area with ST1-DP3 Al-Al.

It shall be noted again that the vibration speed (max: 209.440 m/s) used in this study is far higher than that (max: 1.885 m/s) in reality. Since an impact effect did not occur during the simulation, it is ascertained that the impact effect will not occur at a much lower speed.

4. Results and discussion on impact factors

4.1. Materials

The material was changed from Al-Al to Cu-Cu so that the influence of the material on the microweld changes can be studied. First, DP1 was implemented. As the same vertical displacement was reached, the normal stress became much larger than that for Al-Al. This means that to get the same deformation of the asperities, a larger normal force and a higher US power are needed for Cu-Cu bonding [46,47]. As the horizontal movement started, the microwelds were deformed. At the time of Fig. 13(a), the microweld formed by the larger asperities was about to be broken while the smaller asperity of the wire part was forming a new microweld with the larger asperity of the substrate part. At the end of the leftwards movement (see Fig. 13(b)), the two asperities of the substrate part did not merge into one, which is also different from Al-Al in Fig. 7(c). This is due to the higher stiffness of copper. The final surface topographies are shown in Fig. 13(c). Compared to Fig. 7(g), the two Cu surfaces were less flattened and the asperities

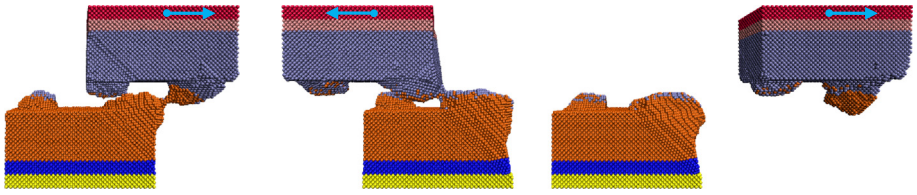

Fig. 13. Breakage and re-formation of microwelds with ST1-DP1 Cu-Cu.

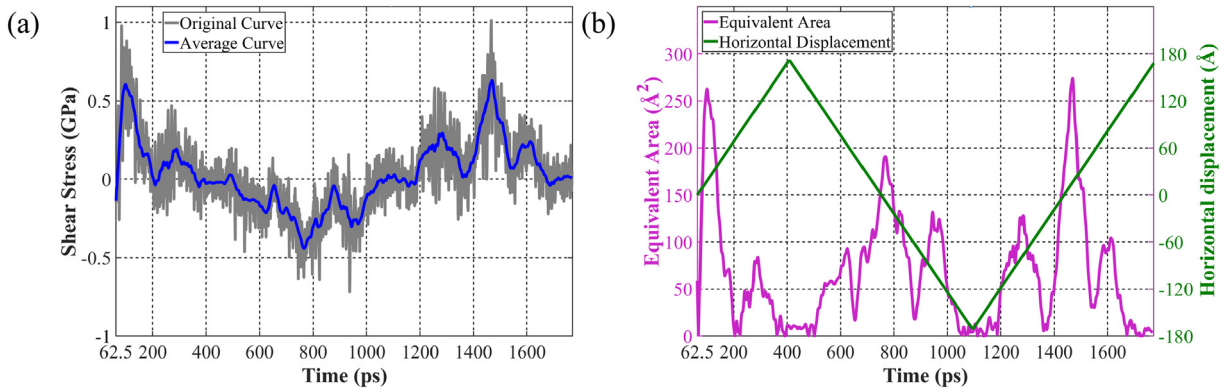

Fig. 14. (a) Shear stress (b) equivalent bonded area with ST1-DP1 for Cu-Cu.

stayed separated. These indicate that a higher stiffness inhibits the change of the surface topographies during vibration.

As shown in Fig. 14(a), the shear stress is significantly larger than that for Al-Al. However, it did not significantly change during the process. The equivalent microweld area (see Fig. 14(b)) in the beginning (262 Å^2) and the ending stages (274 Å^2) are also quite close. As shown in Section 3.1, the equivalent bonded area for Al-Al increased for ~1.35 times from beginning to the end due to the horizontal movement. This indicates that the stiffness of the material negatively influences the microweld area growth caused by horizontal movements.

Similar situations took place for DP2. As shown in Fig. 15(a), a large deformation occurred when the wire part moved to its rightmost position. With the same horizontal displacement, the deformation of the wire part for Al-Al is significantly larger due to the smaller yield stress. At the moment of Fig. 15(b), the larger asperity of the wire part still did not touch the smaller asperity of the substrate part. In the Al-Al process (see Fig. 9(f)), however, the two asperities of the substrate part had formed microwelds with the larger asperity of the wire part in the third vibration cycle. The same situation for Cu-Cu did not happen until the fifth cycle. At the end of the fourth cycle, the two asperities of the wire part and the substrate part were still separated, as in Fig. 15(c).

The shear stress for Cu-Cu under ST1-DP2 are much larger than that for Al-Al. During the four vibration cycles, however, no big changes were found on the shear stress and the microweld area in Fig. 16. This is in accordance to the little microweld changes observed in Fig. 15. Comparably, an apparent increment of the shear stress and bonded area can be found for Al-Al in Section 3.2. In the last vibration cycle, due to the large stress induced distortion of the wire part, the bonded area of Al-Al was smaller than that of Cu-Cu. This shows that the stiffness of the material has a negative effect on the microweld growth. To obtain a similar microweld area, more vibration cycles would be needed. Apart from the oxide removal process, this could be another reason why copper wire bonding takes a longer time than aluminum wire bonding [47].

The microweld changes for Cu-Cu under DP3 are shown in Fig. 17. First, the large deformation of the substrate part as marked in Fig. 11 (b) did not occur for Cu-Cu. Under the scrubbing (constant movement

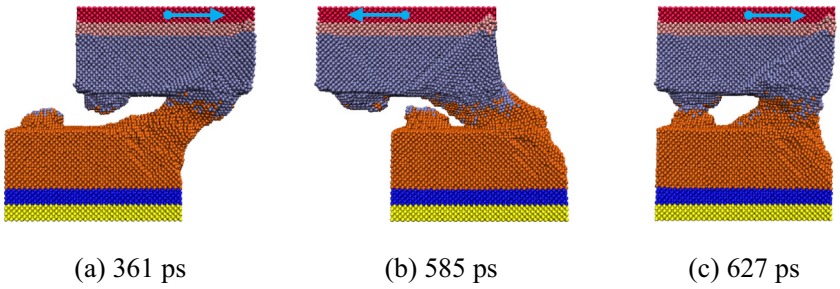

Fig. 15. Breakage and re-formation of microwelds with ST1-DP2 Cu-Cu.

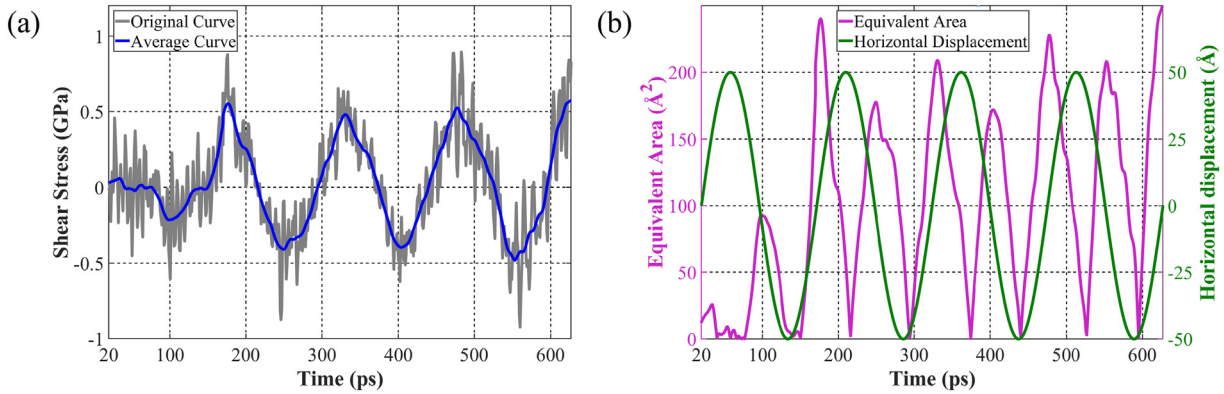

Fig. 16. (a) Shear stress (b) equivalent bonded area with ST1-DP2 Cu-Cu.

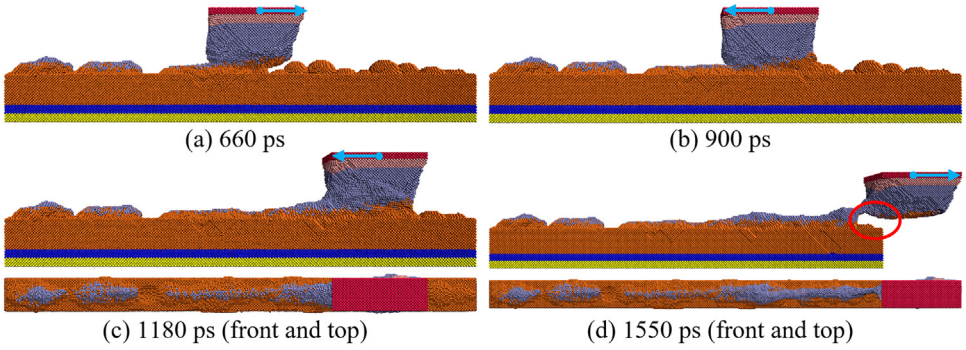

Fig. 17. Breakage and re-formation of microwelds with ST1-DP3 Cu-Cu.

and vibration) of the wire part, the substrate surface was smoothened. As seen from Fig. 17(a) to (c), there were no large observable differences from those for Al-Al. From Fig. 17(c) to (d), large amounts of atoms from the wire part remained on the substrate part. This shows why the microweld area counting by the observation method mentioned in Introduction is inaccurate [2,14]. Compared to that for Al-Al, the microweld between the wire part and the substrate part was disconnected at an earlier stage of the moving route. As shown in Fig. 17 (d), the wire part did not touch the marked area of the substrate. In general, the deformation of the Cu substrate was less substantial than that of the Al substrate and the resulting surface was rougher.

A gradual increase of the shear stress and the microweld area can be observed in both Al-Al and Cu-Cu cases, except the first vibration cycle for Cu-Cu as in Fig. 18. The largest equivalent bonded area for Cu-Cu was reached during the 5th vibration cycle and was kept constant until the 8th cycle when the bonded area for Al-Al reached its peak value. In addition, the peak value of the bonded area for Cu-Cu was smaller than that for Al-Al. These indicate that the larger stiffness of Cu prevented the deformation of the bonding partners and the further growth of the microweld area. Nevertheless, the shear stress of the Cu-Cu microweld (peak value: 0.838 GPa) was larger than that of the Al-Al microweld, as compared between Figs. 12(a) and 18(a).

In this section, it is shown that a high stiffness has a negative effect on the topography change and microweld growth. To reach a similar level of microweld area under the same displacement pattern, more vibration cycles are required.

4.2. Surface topography

In different areas of the wire or substrate surface, different topographies exist. To investigate the influence of the surface topography on shear stress and microweld changes, three different topographies were established as in Fig. 19. In ST2, the radius of all asperities was set at 15 Å and the two asperities of the wire part were not aligned with those of the substrate part. The two asperities of the substrate part in ST3 were placed together as in (b). In ST4, two pits with a radius

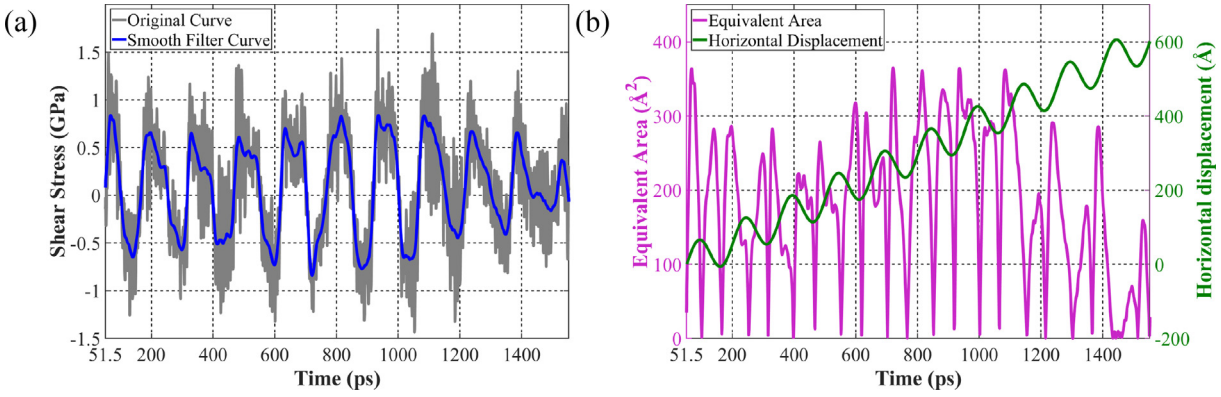

Fig. 18. (a) Shear stress (b) equivalent bonded area with ST1-DP3 Cu-Cu.

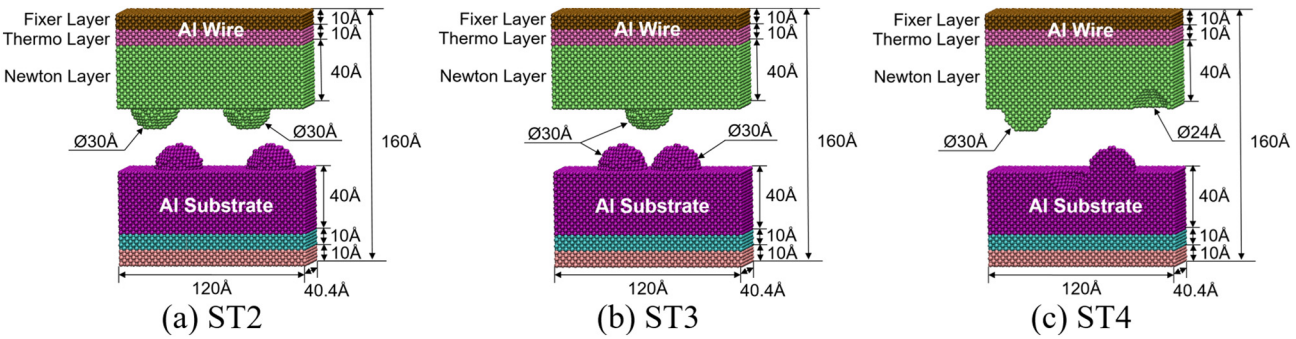

Fig. 19. Geometries of different surface topographies for Al-Al.

of 12 Å were created on both surfaces. To make the two surfaces of ST4 come into contact, a 30 Å downwards movement was applied. Since the wire and the substrate came into contact during the second vibration cycle, an additional vibration cycle (five cycles in total while four cycles for the others) was added.

The final topographies after DP1 for ST2–4 are shown in Fig. 20(a)–(c), respectively. In the case of ST2, only a small volume of the asperities of the wire and substrate part came into contact due to the small radius of the asperities. No significant change of the topographies was observed in (a). The misalignment of the asperities insignificantly influenced the microweld changes. Compared to ST1-DP1, the significant role of the larger asperities is demonstrated. The formation, deformation and breakage of the larger microweld constituted by the larger asperities greatly changed the topographies of both surfaces. This is further validated by the small changes in (b). When there were only three small asperities, the topographies after four vibration cycles were nearly the same as those before vibration. In the case of ST4 where the wire and pad surfaces were much closer than those in the other cases, the final topographies were totally changed. As shown in (c), the pits on both the wire and the pad were filled up and the microweld was still connected after the second-round rightwards moving despite the large deformation.

The changes of the shear stress and the equivalent bonded area for ST2–4 under DP1 are plotted in Fig. 21. For ST2-DP1, since only small areas of the asperities were in contact after the pressing, the largest shear stress was only 0.246 GPa (0.325 GPa for ST1-DP1 at the same moment). As the horizontal movement continued, the shear stress decreased (see Fig. 21(a)), which indicated that the effective reaction volume of the Newton layer became even smaller. The largest equivalent bonded area was smaller than 175 $Å^2$ (see Fig. 21(b)), which was only half of that for ST1-DP1. As has been shown in Fig. 20(b), the surface topographies of ST3 did not significantly change before and after the vibration. Thus, the shear stress and the bonded area in Fig. 21(c)–(d) were small and did not significantly change. A much larger area was connected in ST4 but mainly due to the smaller distance between the two surfaces. In Fig. 21(e)–(f), obvious increments of the shear stress and the bonded area were illustrated. The peak values were about 1.5 times larger than those for ST1-DP1. The impact of the approaching distance will be further discussed in Section 4.3.

Fig. 20(d)–(f) shows the final shape of the microwelds for ST2–4 under DP2. In the case of ST2, all the asperities merged into a single microweld as in (d). The wire part was distorted by the vibration. For ST3, the three asperities soon merged together into one microweld after one vibration cycle while the last three vibration cycle did not change the final shape of the microweld, as shown in (e). In this case, the wire part was not distorted. For ST4, the two lumps formed a microweld while both the pits were not filled up until the fourth vibration cycle. During the fifth vibration cycle, the microweld area was enlarged and the two pits vanished, as shown in (f).

The shear stress and the equivalent bonded area of ST2–4 under DP2 are shown in Fig. 22. As shown in Fig. 22(a), after the merge of the four asperities, the peak shear stress (~0.18 GPa) and microweld area (~125 $Å^2$) stayed at the same level, which was significantly smaller than that for ST1-DP2. This is in accordance to the observation in Fig. 20(d) where the microweld did not greatly change. The changes of the microweld for ST3 were similar to those for ST2 despite the existence of only three asperities. As shown in Fig. 22(c) (d), the peak values of the shear stress and the bonded area were kept at a level which was about 3/4 of those for ST2. As for ST4, large increments of the shear stress and the bonded area were found in the fifth vibration cycle (see Fig. 22(e) (f)). The final values were significantly larger than those of the other cases due to the smaller distance between the two surfaces.

In general, ST2–4 can demonstrate two conditions: 1) the asperities are not effectively deformed for a smooth surface; 2) the local small asperities are not well connected as the surrounding large asperities are not effectively deformed for a rough surface. Thus, the deformation of asperities, especially large asperities, significantly influences the shear stress and the bonded area. In actual bonding process, effective deformation of asperities usually occurs due to the softening effect. When this does not happen, the bonding quality becomes low [9,45].

4.3. Approaching distance

For the same initial surface condition, the deformation of the asperities is different when different US powers and normal forces are applied. The deformation of asperities is supposed to greatly influence the microweld changes as well as the final topographies. To study this influence, a 5 Å further vertical displacement was imposed in the three DPs.

Since a 5 Å further downwards movement was imposed, the normal stress was larger and the deformation of the Newton layer became more substantial. From Fig. 23(a) to (b), there is no large difference during the

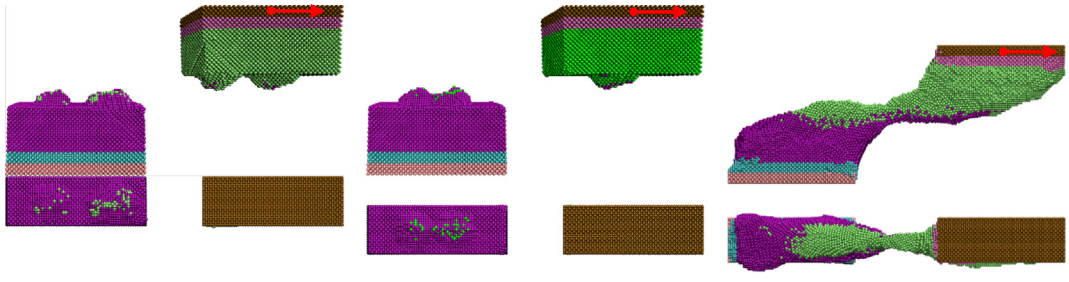

(a) ST2-DP1 (Front and top) (b) ST3-DP1 (Front and top) (c) ST4-DP1 (Front and top)

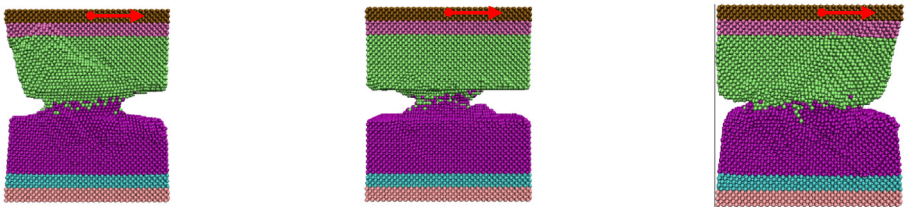

(d) ST2-DP2 (e) ST3-DP2 (f) ST4-DP2

Fig. 20. Final status of microwelds with different STs and DPs for Al-Al.

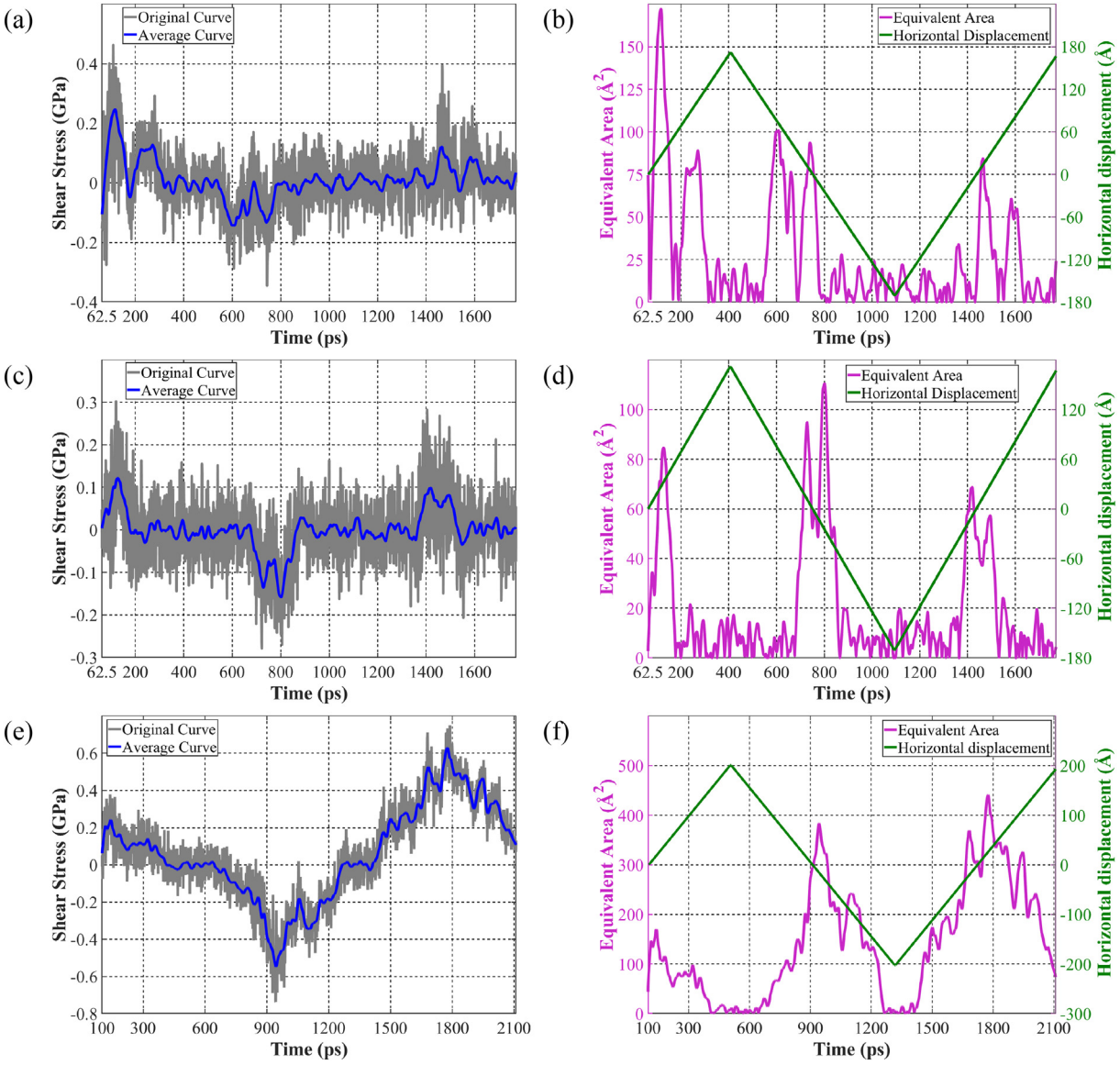

Fig. 21. (a) Shear stress (b) equivalent bonded area with ST2-DP1 Al-Al; (c) shear stress (d) equivalent bonded area with ST3-DP1 Al-Al; (e) shear stress (f) equivalent bonded area with ST4-DP1 Al-Al.

rightwards movement, compared to ST1-DP1 in Fig. 6. When the wire moved back as in Fig. 23(c) (d), the whole surfaces were connected together. Compared to ST1-DP1, the joining of the whole surfaces was finished in advance for 630 ps. Since the joining became stronger, more dislocations or even the geometry distortion of the wire part and the substrate part can be observed in (e) (f) during the second round of rightwards movement. With the same horizontal displacement, the microweld was finally not broken as in (f). This shows that as a microweld grows, it can be strong enough to withstand the vibration induced shear stress; under the same vibration amplitude, the microweld will not be broken.

The differences from ST-DP1 under the 15 Å vertical movement are also shown in the shear stress and the equivalent bonded area in Fig. 24. The largest shear stress under the 15 Å vertical movement was around 0.4 GPa. With the 5 Å further pressing, this value had been reached in the beginning as in Fig. 24(a) and it was further enhanced to ~0.56 GPa. The enhancement was also shown in the equivalent bonded area which increased from 308 Å^2 to ~390 Å^2. Thus for DP1, this larger approaching distance had a significant influence on the topography change and microweld growth.

A further 5 Å vertical displacement was also imposed on DP2. The total 20 Å vertical movement was finished within two vibration cycles. Therefore, five vibration cycles were applied in total. As shown in Fig. 25(a), the two asperities of the substrate part had been merged into a large single asperity, which did not occur in the ST1-DP2 case. At the time of (b), the four initial asperities joined together and the joining stayed until the end of the simulation, as can be seen in (c).

Compared to Fig. 10, the shear stress and the equivalent bonded area were enhanced by the 5 Å further approaching distance as shown in Fig. 26. Right after the vertical movement, the microweld area had reached 164 Å^2. After the merging of all asperities, the shear stress increased to 0.4 GPa and the microweld area increased to 281 Å^2, which were 21% larger than those with 15 Å approaching distance. This further indicates the significant role of the vertical movement.

When the 5 Å further approaching distance was imposed on ST1-DP3, the wire surface was totally mated with the substrate surface in a short time, as shown in Fig. 27(a). As the constant horizontal movement continued, the wire part was extensively stretched as in Fig. 27(b). At the time of Fig. 27(c), the Newton layer of the wire part was almost detached from the thermo layer. In the remaining process, large amounts

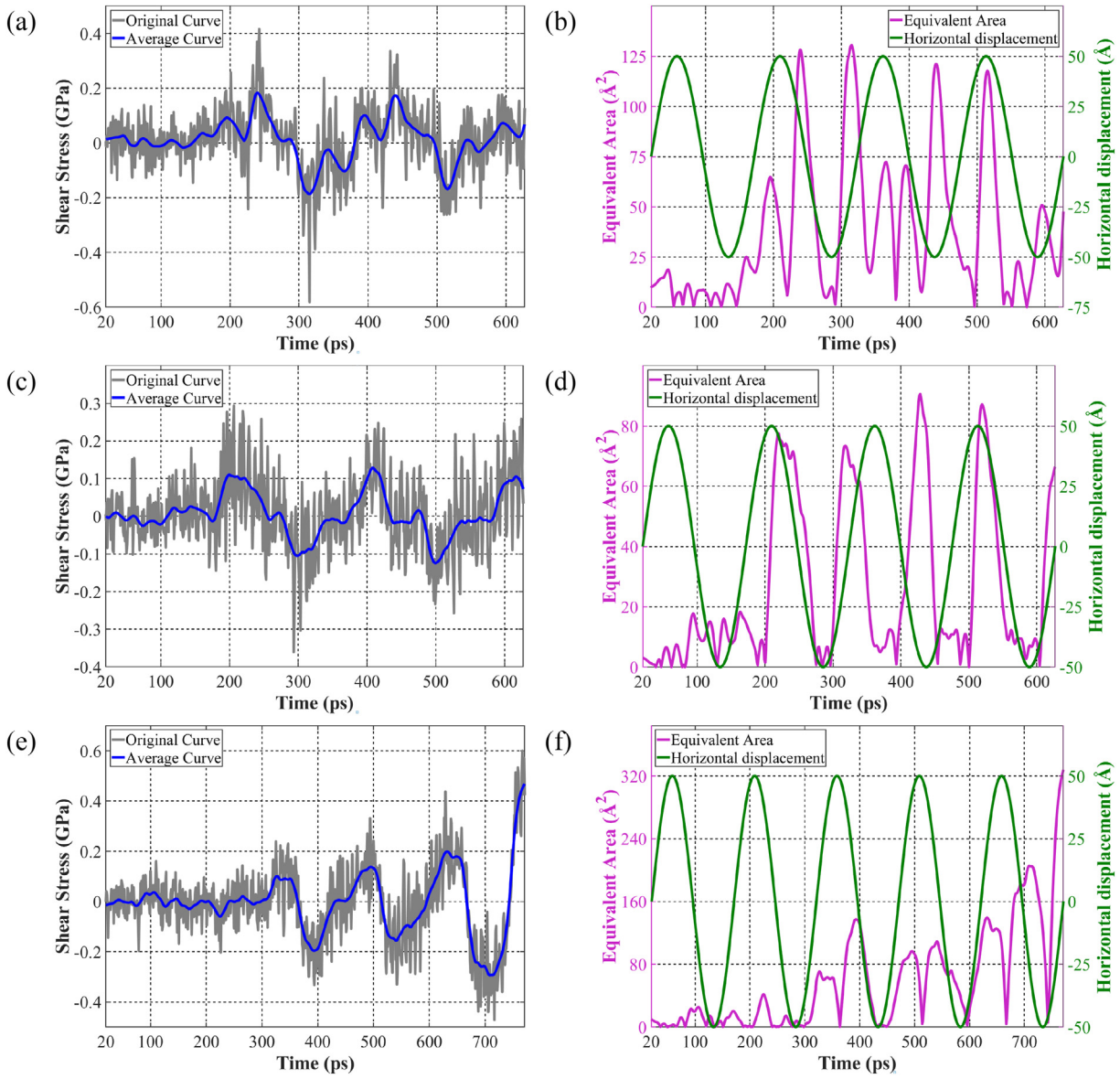

Fig. 22. (a) Shear stress (b) equivalent bonded area with ST2-DP2 Al-Al; (c) shear stress (d) equivalent bonded area with ST3-DP2 Al-Al; (a) shear stress (b) equivalent bonded area with ST4-DP2 Al-Al.

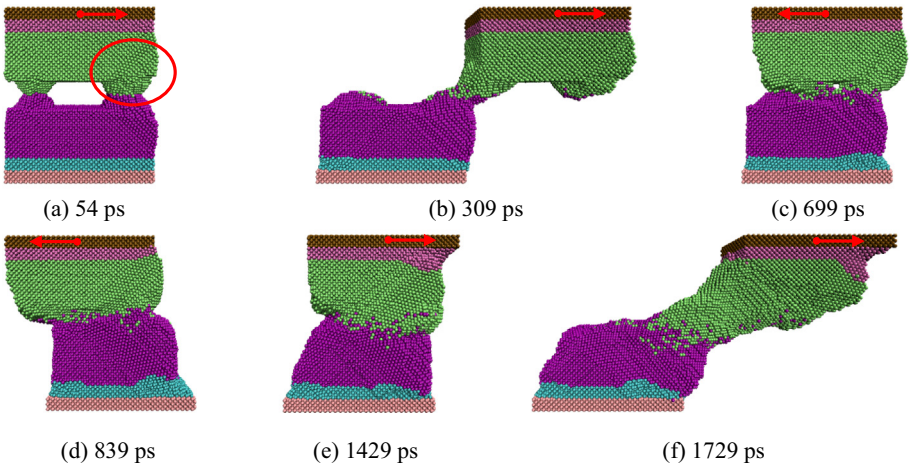

Fig. 23. Breakage and re-formation of microwelds with ST1-DP1 Al-Al but with a 5 Å further approaching distance.

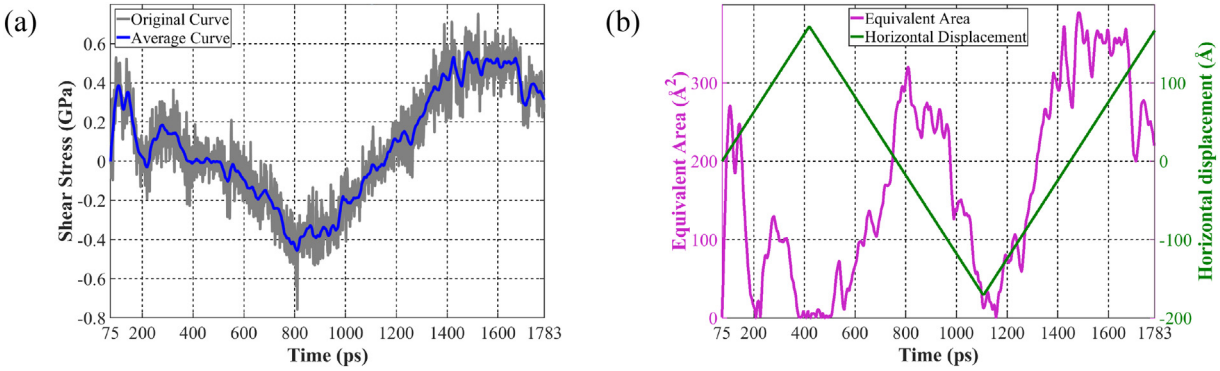

Fig. 24. (a) Shear stress (b) equivalent bonded area with ST1-DP1 Al-Al but with a 5 Å further approaching distance.

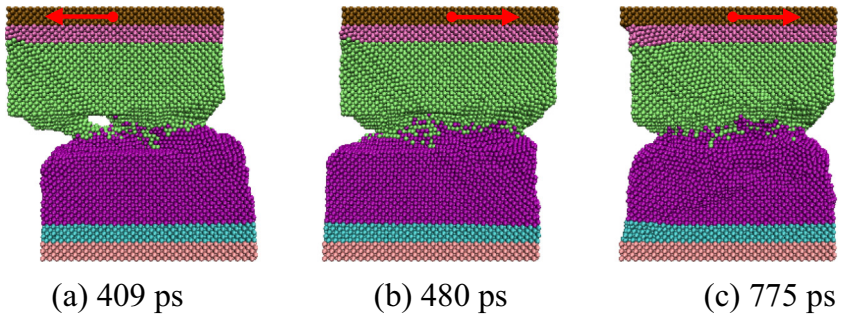

Fig. 25. Breakage and re-formation of microwelds with ST1-DP2 Al-Al but with a 5 Å further approaching distance.

of atoms from the wire Newton layer stuck on the substrate surface and the wire part became smaller. Finally, a "bottle-neck" was formed as shown in Fig. 27(d). Compared to ST1-DP3, the significance of the approaching distance was demonstrated.

As shown in Fig. 28, the shear stress and the equivalent bonded area greatly increased in the first two and half vibration cycles. Due to the larger approaching distance, the values were significantly larger than those under ST1-DP3. For example, during this period, the bonded area with the 20 Å vertical movement reached 545 $Å^2$ while only 313 $Å^2$ was achieved with the 15 Å vertical movement. In the following process, the Newton layer of the wire part was extensively stretched due to the large stress. Atoms from the wire Newton layer were transferred to the substrate part and the connection between the Newton layer and the thermo layer became weaker. Thus in Fig. 28, gradual decrements in the shear stress and the equivalent bonded area were observed in the rest vibration cycles.

In this section, under different DPs, the positive effect of the approaching distance on the enhancement of the shear stress and the bonded area was revealed, which is in agreement with the statement of Murali et al. [45]. As discussed before, the approaching distance corresponds to the normal force and US power. The normal force produces the normal stress on the asperities and transfers the US energy to the asperities [6]. The US power provides the energy for the softening effect and generates vibration. In other words, US power significantly influences the approaching distance and vibration. Thus, in a certain range, a larger normal force and a higher US power could enhance the bonding quality.

4.4. Vibration amplitude

The vibration during wire bonding is generated by the US power and different powers produce different vibration amplitudes. In Section 3, a

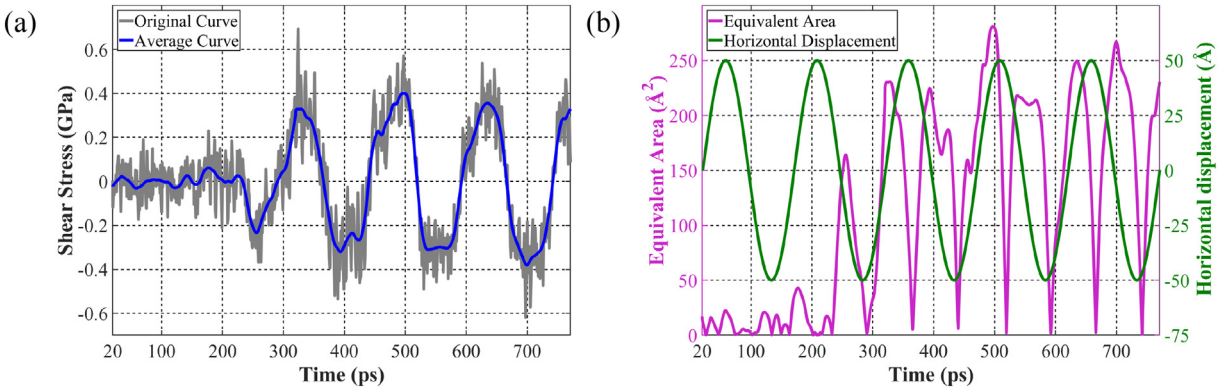

Fig. 26. (a) Shear stress (b) equivalent bonded area with ST1-DP2 Al-Al but with a 5 Å further approaching distance.

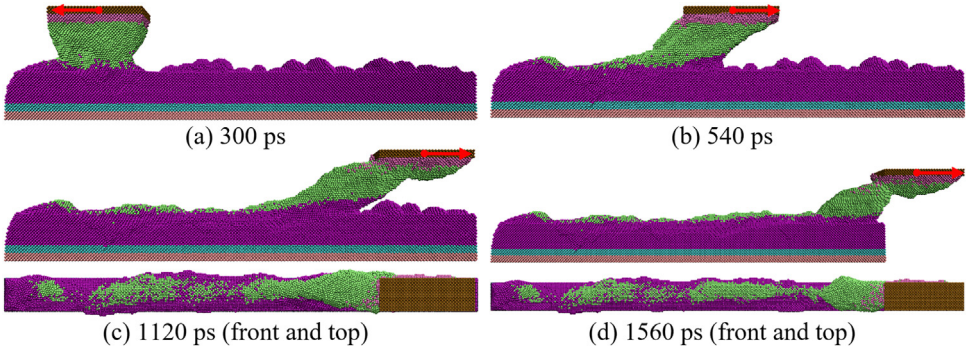

Fig. 27. Breakage and re-formation of microwelds with ST1-DP3 Al-Al but with a 5 Å further approaching distance.

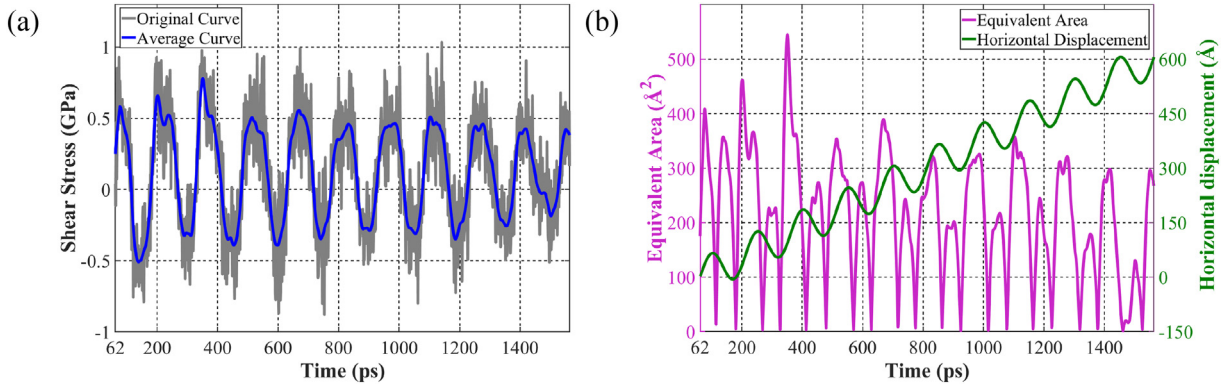

Fig. 28. (a) Shear stress (b) equivalent bonded area with ST1-DP3 Al-Al but with a 5 Å further approaching distance.

50 Å vibration amplitude was used for DP2 and DP3. In this section, the vibration amplitude was increased to 80 Å to investigate the influence of the vibration amplitude on the microweld changes.

Fig. 29 shows the microweld changes with ST1-DP2 but with an 80 Å vibration amplitude. As shown in (a), the two asperities of the substrate part were already merged together at 280 ps while this did not occur until the last vibration cycle with ST1-DP2. Due to the larger vibration amplitude, the microweld was almost broken as shown in (b), which did not happen for ST1-DP2. Finally, all the four asperities merged into one microweld, as show in (c). This indicates that a large vibration amplitude makes the microweld change faster and could sometimes even cause a detrimental effect.

With the 80 Å vibration amplitude, increments of the shear stress and the bonded area were observed in Fig. 30. The values, however, were not enhanced by the larger vibration amplitude. This shows that a larger vibration amplitude does not necessarily increase the shear stress and the microweld area.

The vibration amplitude for ST1-DP3 was also increased to 80 Å and the corresponding microweld changes are shown in Fig. 31. At the moment of (a), the wire surface totally mated with the substrate surface, which is similar to that with ST1-DP3. The difference is marked in the red ellipse where the substrate surface was smoothened. From (a) to (b), large amounts of atoms from the wire Newton layer were left on the substrate surface and filled up many valleys. The connected area greatly decreased and the few small asperities of the substrate surface changed to two large asperities. As shown in (c), the wire part was disconnected with the substrate part. When the wire part vibrated back, the microweld was re-formed. These changes, which did not take place with ST1-DP3, show that too large a vibration amplitude has a negative effect on the microweld growth under DP3. This, however, was not true when the back side of the wire part is supplemented by other wire materials. This will be shown in the last subsection.

The changes of the shear stress and the equivalent bonded area with ST1-DP3 under the 80 Å vibration amplitude are shown in Fig. 32. Before the middle of the process, the shear stress and the bonded area increased to 0.629 GPa and 441 Å^2, respectively. Due to the transfer of the atoms from the wire part to the substrate part, the shear stress and the

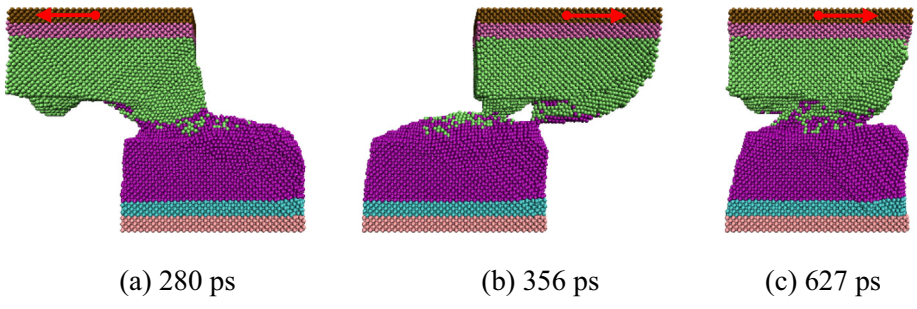

Fig. 29. Breakage and re-formation of microwelds with ST1-DP2 Al-Al but with an 80 Å vibration amplitude.

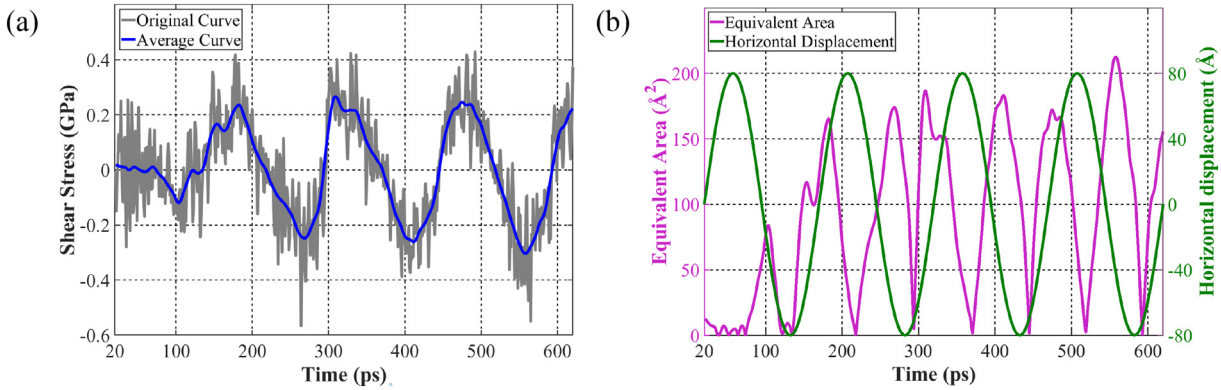

Fig. 30. (a) Shear stress (b) equivalent bonded area with ST1-DP2 Al-Al but with an 80 Å vibration amplitude.

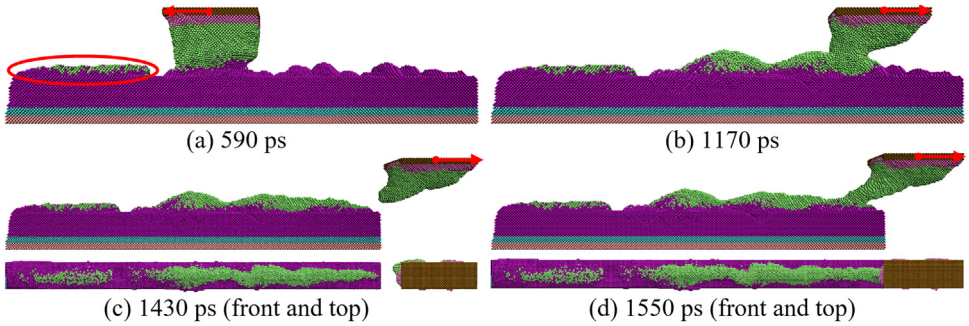

Fig. 31. Breakage and re-formation of microwelds with ST1-DP3 Al-Al but with an 80 Å vibration amplitude.

bonded area decreased afterwards. Compared to ST1-DP3, the shear stress and the bonded area reached their peak values in a shorter time.

The results show that a large vibration amplitude makes the microweld change faster while a large vibration amplitude does not necessarily increase the shear stress and the microweld area. In actual bonding process, a higher US power might cause more substantial deformation of asperities. However, it could also break the existing microwelds when the shear stress increases [7]. As a result, a middle level of US power is usually preferred [6,48].

4.5. Scaling

Compared to the wire bonding in reality, the models above have a much smaller dimension. To study the scaling effect on the simulation results, each of the three dimensions of ST1 was magnified by three times. The magnified model has 1.05 million atoms. Despite the magnification, the dimensions of the asperities are still only comparable to the uncommonly used surface roughness [7,9]. Therefore, the results in this work are only used to deduce the microweld and surface topography changes in reality.

Fig. 33(a) and (b) shows the microweld changes during the first rightwards movement. There was nearly no difference compared to the unscaled model in Fig. 6. As the wire part moved to the left, it gripped large amounts of atoms from the larger asperity of the substrate part, as shown in Fig. 33(c). With further displacement to the moment of Fig. 33(d), the space between the two asperities of the wire part was fulfilled with the atoms from the substrate. The microweld changes during the second rightwards movement are shown in Fig. 33(e)–(g). Even though the topography changes of the scaled model are different from those of the unscaled model, similar microweld formation, deformation and breakage took place which led to a significant change of the topographies. Thus, it is assumed that in wire bonding processes,

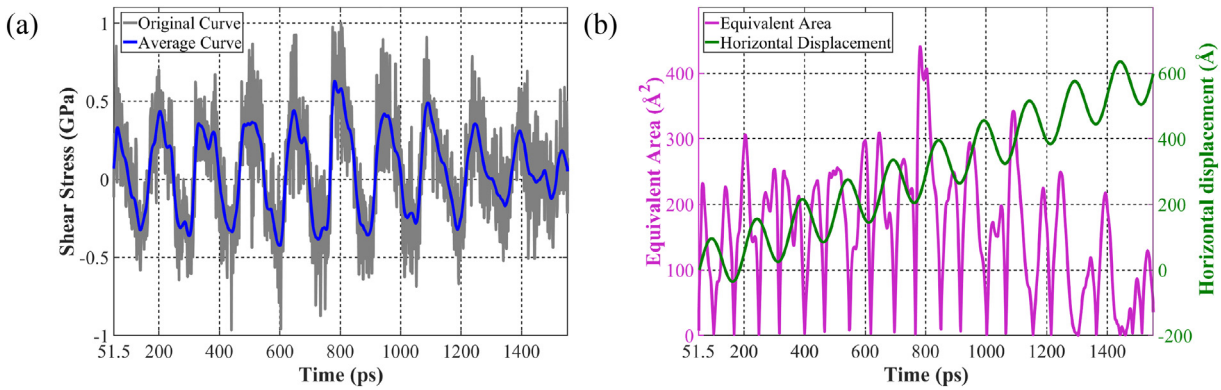

Fig. 32. (a) Shear stress (b) equivalent bonded area with ST1-DP3 Al-Al but with an 80 Å vibration amplitude.

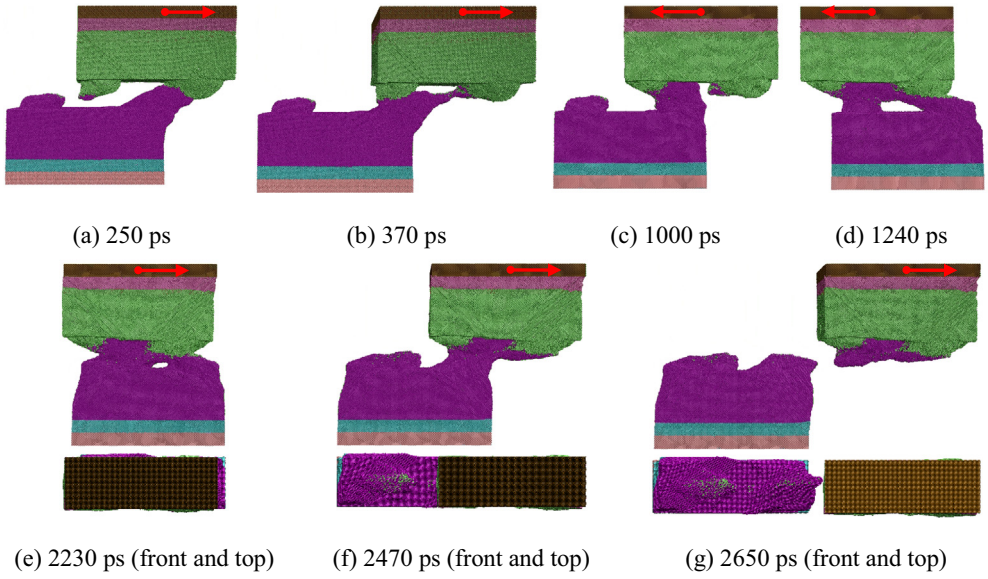

Fig. 33. Breakage and re-formation of microwelds with magnified ST1-DP1 Al-Al.

the normal force (vertical movement) and vibration cause microweld formation, deformation and breakage; in different locations of the interface, these changes are different; the topographies are greatly changed in all locations of the interface.

As the rightwards movement starts, the shear stress soon reached its maximal value (0.295 GPa), as shown in Fig. 34(a). Due to the gripping of the substrate atoms, the shear stress did not increase in the following process, which is different from that of the unscaled model in Fig. 8. The curve in Fig. 34(b) shows a maximal equivalent bonded area of 1858 $Å^2$. This is about 9 times higher than that of the unscaled model at the same time and is in accordance to the scaling factor of 3.

The microweld changes of the magnified ST1 model under DP2 are shown in Fig. 35. During the first two vibration cycles, the two microwelds were largely deformed as shown in Fig. 35(a). In the third cycle, all four asperities merged into a large microweld (see Fig. 35(b)). With a further vibration cycle, as in Fig. 35(c), both the wire part and the substrate part were distorted.

Fig. 36(a) and (b) shows that the shear stress and the equivalent bonded area gradually increased along with time, respectively. This is due to the deformation of the thermo-layer and the Newton layer of the wire part. The x-dimension (horizontal) of these two layers shrunk while their z-dimension (vertical) was enlarged. This made the two Newton layer surfaces even closer and thus a larger area was bonded.

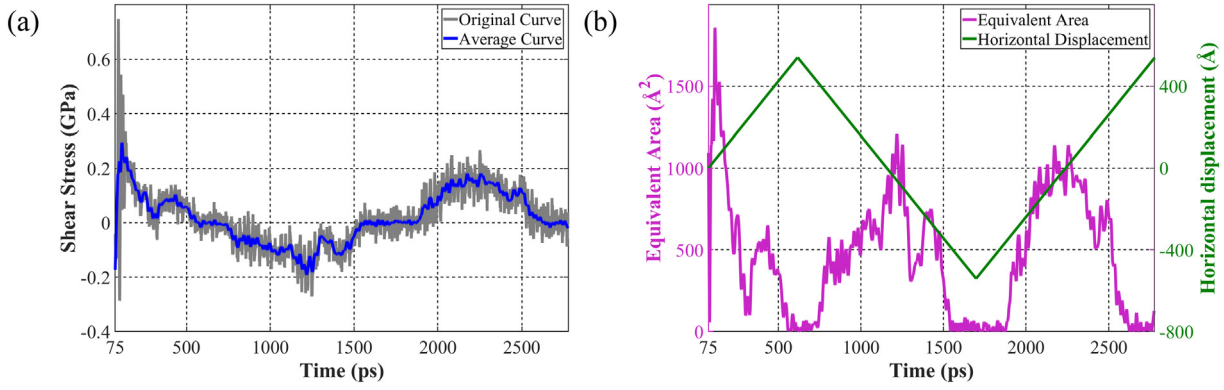

Fig. 34. (a) Shear stress (b) equivalent bonded area with magnified ST1-DP1 Al-Al.

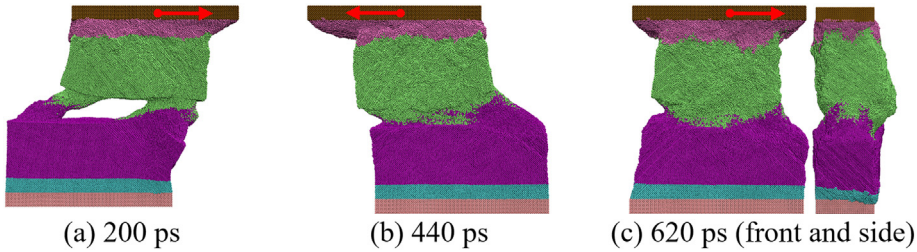

Fig. 35. Breakage and re-formation of microwelds with magnified ST1-DP2 Al-Al.

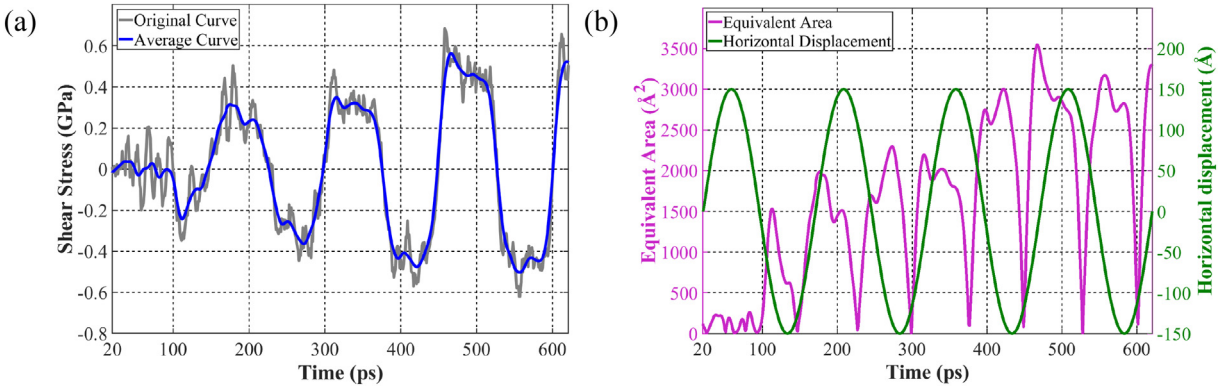

Fig. 36. (a) Shear stress (b) equivalent bonded area with magnified ST1-DP2.

The scaling for ST1-DP3 was made differently. Only the x-dimension of the wire part was extended for five times and the results are shown in Fig. 37. Under the current configuration, the two surfaces mated together into a single microweld after the interaction among tens of asperities, as shown from (a) to (b). As the wire part continued to move rightwards, the microweld area decreased. From (c), it can be seen that the large deformation of the wire part took place before the breakage of this large microweld. Large amounts of atoms from the substrate Newton layer were taken away by the wire part. Finally, the surface topographies were significantly changed, especially the wire part.

Both the shear stress and the equivalent bonded area first increased until the two surfaces totally mated together and then decreased, which are shown in Fig. 38.

With a scaling factor of 3 or 5 at one dimension, similar formation, deformation and breakage behaviors of microwelds still took place.

5. Conclusions

Based on the simulation results, the mechanism of microweld changes including the formation, deformation and breakage of microwelds can be summarized as:

- Microwelds can be formed and broken in an extremely short time. The formation and breakage of microwelds take place continuously during the bonding process.
- The local positions where old microwelds have been broken still offer the opportunity for the formation of new microwelds, even with the same asperities.
- The constant horizontal movement of the wire significantly changes the surface topographies.
- Under the same conditions, a high stiffness of the materials has a negative effect on the microweld growth.

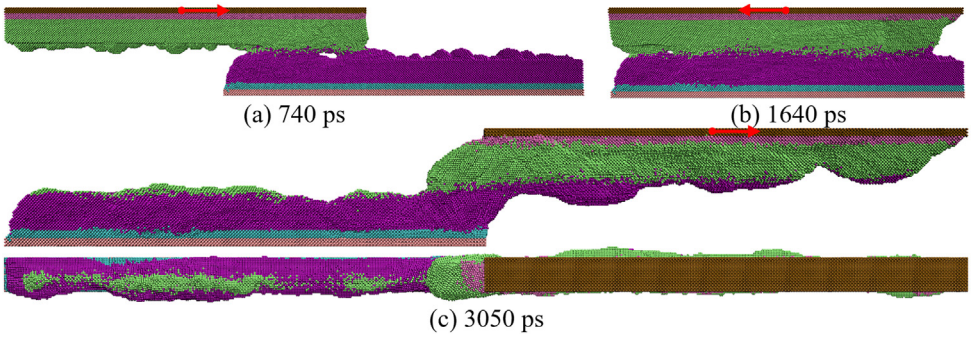

Fig. 37. Breakage and re-formation of microwelds with extended ST1-DP3 Al-Al.

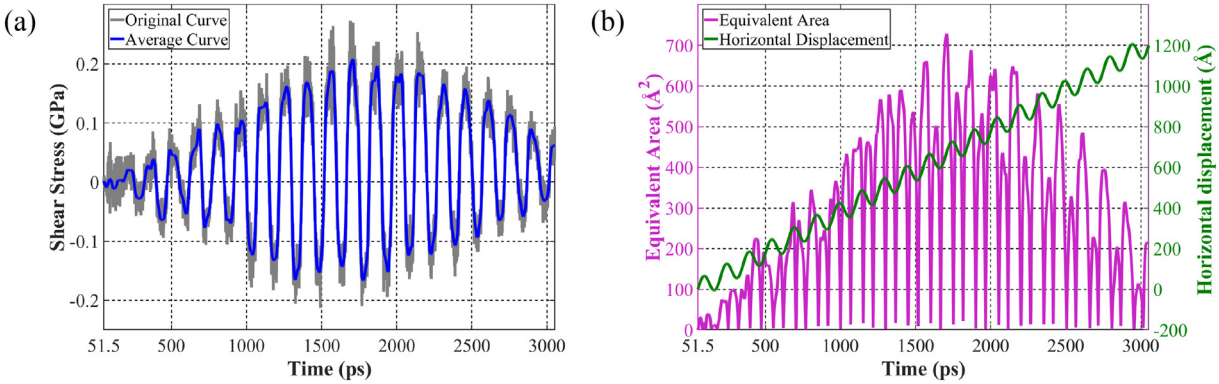

Fig. 38. (a) Shear stress (b) equivalent bonded area with extended ST1-DP3 Al-Al.

- A large approaching distance or a large deformation of asperities (especially large asperities) significantly helps the microweld growth.
- A larger vibration amplitude makes the microweld changes faster while this large vibration amplitude does not necessarily increase the shear stress and the microweld area.

CRediT authorship contribution statement

Yangyang Long: Conceptualization, Methodology, Software, Formal analysis, Writing - original draft, Writing - review & editing, Supervision. **Bo He:** Methodology, Software, Resources, Writing - review & editing. **Weizhe Cui:** Software, Formal analysis. **Yuhang Ji:** Software, Formal analysis. **Xiaoying Zhuang:** Methodology, Supervision. **Jens Twiefel:** Conceptualization, Writing - review & editing, Supervision, Funding acquisition.

Declaration of competing interest

The authors declare that they have no known competing financial interests or personal relationships that could have appeared to influence the work reported in this paper.

Acknowledgements

The financial support from DFG (Deutsche Forschungsgemeinschaft) program (TW75/8-1|WA564/40-1) is gratefully acknowledged. The publication of this article was funded by the Open Access Publishing Fund of Leibniz Universität Hannover.

Data availability

The raw and processed data required to reproduce these results are available by contacting the authors.

Appendix A. Supplementary data

Animations for ST1-DP1 Al-Al, ST1-DP2 Al-Al, ST1-DP3 Al-Al, ST1-DP2 Cu-Cu, ST1-DP1 Al-Al with 20 Å approaching distance and ST1-DP3 Al-Al with 80 Å vibration amplitude are supplemented. The other animations are available on request. Supplementary data to this article can be found online at https://doi.org/10.1016/j.matdes.2020.108718.

References

[1] G.G. Harman, Wire Bonding in Microelectronics, third ed. McGraw-Hill, New York, USA, 2010.
[2] Y. Long, J. Twiefel, J. Wallaschek, A review on the mechanisms of ultrasonic wedge-wedge bonding, J. Mater. Process. Technol. 245 (2017) 241–258.
[3] F. Osterwald, Verbindungsbildung beim Ultraschall-Drahtbonden: Einfluß der Schwingungs-parameter und Modellvorstellungen, Doctoral dissertation Technical University of Berlin, 1999.
[4] Y. Long, F. Dencker, A. Isaak, J. Hermsdorf, M. Wurz, J. Twiefel, Self-cleaning mechanisms in ultrasonic bonding of Al wire, J. Mater. Process. Technol. 258 (2018) 58–66.
[5] H. Gaul, M. Schneider-Ramelow, H. Reichl, Analysis of the friction processes in ultrasonic wedge/wedge-bonding, Microsyst. Technol. 15 (2009) 771–775.
[6] Y. Long, F. Schneider, C. Li, J. Hermsdorf, J. Twiefel, J. Wallaschek, Quantification of the energy flows during ultrasonic wire bonding under different process parameters, Int. J. Precis. Eng. Manuf.-Green Technol. 6 (2019) 449–463.
[7] Y. Long, F. Dencker, A. Isaak, C. Li, F. Schneider, J. Hermsdorf, M. Wurz, J. Twiefel, J. Wallaschek, Revealing of ultrasonic wire bonding mechanisms via metal-glass bonding, Mater. Sci. Eng. B 236 (2018) 189–196.
[8] F. Blaha, B. Langenecker, Dehnung von Zink-Kristallen unter Ultraschalleinwirkung, Naturwissenschaften 42 (1955) 556.
[9] J.E. Krzanowski, N. Murdeshwar, Deformation and bonding processes in aluminum ultrasonic wire wedge bonding, J. Electron. Mater. 19 (1990) 919–928.
[10] U. Geissler, M. Schneider-Ramelow, H. Reichl, Hardening and softening in AlSi1 bond contacts during ultrasonic wire bonding, IEEE Trans. Compon. Packag. Technol. 32 (2009) 794–799.
[11] U. Geissler, J. Funck, M. Schneider-Ramelow, H.J. Engelmann, I. Rooch, W.H. Müller, H. Reichl, Interface formation in the US-wedge/wedge-bond process of AlSi1/CuNiAu contacts, J. Electron. Mater. 40 (2011) 239–246.
[12] M. Maeda, K. Yamane, S. Matsusaka, Y. Takahashi, Relation between vibration of wedge-tool and adhesion of wire to substrate during ultrasonic bonding, Q. J. Japan Weld. Soc. 27 (2009) 200s–203s.
[13] J.L. Harthoorn, Ultrasonic Metal Welding, Doctoral dissertation Technical University of Braunschweig, 1978.
[14] H. Seppänen, R. Kurppa, A. Meriläinen, E. Hæggström, Real time contact resistance measurement to determine when microwelds start to form during ultrasonic wire bonding, Microelectron. Eng. 104 (2013) 114–119.
[15] Y. Zhou, X. Li, N.J. Noolu, A footprint study of bond initiation in gold wire crescent bonding, IEEE Trans. Compon. Packag. Technol. 28 (2005) 810–816.
[16] I. Lum, M. Mayer, Y. Zhou, Footprint study of ultrasonic wedge-bonding with aluminum wire on copper substrate, J. Electron. Mater. 35 (2006) 433–442.
[17] H. Ji, M. Li, C. Wang, J. Guan, H.S. Bang, Evolution of the bond interface during ultrasonic Al–Si wire wedge bonding process, J. Mater. Process. Technol. 182 (2007) 202–206.
[18] J. Grigoraschwili, W. Scheel, M. Thiede, Charakterisierung von Ultraschall-Schweißverbindungen durch Messen des elektrischen Durchgangswiderstands, Schweiítechnik, 34, 1984 468–470.
[19] S. Goel, X. Luo, A. Agrawal, R.L. Reuben, Diamond machining of silicon: a review of advances in molecular dynamics simulation, Int. J. Mach. Tools Manuf. 88 (2015) 131–164.
[20] X. Guo, Q. Li, T. Liu, R. Kang, Z. Jin, D. Guo, Advances in molecular dynamics simulation of ultra-precision machining of hard and brittle materials, Front. Mech. Eng. 12 (2017) 89–98.
[21] J. Li, W. Meng, K. Dong, X. Zhang, W. Zhao, Study of effect of impacting direction on abrasive nanometric cutting process with molecular dynamics, Nanoscale Res. Lett. 13 (2018) 11.
[22] P. Zhou, X. Shi, J. Li, T. Sun, Y. Zhu, Z. Wang, J. Chen, Molecular dynamics simulation of SiC removal mechanism in a fixed abrasive polishing process, Ceram. Int. 45 (2019) 14614–14624.
[23] V.T. Nguyen, T.H. Fang, Material removal and interactions between an abrasive and a SiC substrate: a molecular dynamics simulation study, Ceram. Int. 46 (2020) 5623–5633.
[24] S. James, M. Sundaram, A molecular dynamics simulation study of material removal mechanisms in vibration assisted nano impact-machining by loose abrasives, J. Manuf. Sci. Eng.-T. ASME 139 (2017), 081014.
[25] W. Zhai, D. Yang, N. Gong, Molecular dynamics simulation of polishing process of silicon carbide under ultrasonic vibration conditions, J. Shanghai Jiaotong Univ. 52 (2018) 599–603.
[26] T. Yu, Z. Wang, X. Guo, P. Xu, J. Zhao, L. Chen, Effect of ultrasonic vibration on polishing monocrystalline silicon: surface quality and material removal rate, Int. J. Adv. Manuf. Technol. 103 (2019) 2109–2119.
[27] H. Dai, J. Chen, G. Liu, A numerical study on subsurface quality and material removal during ultrasonic vibration assisted cutting of monocrystalline silicon by molecular dynamics simulation, Mater. Res. Express 6 (2019), 065908.
[28] T.Q. Vo, B.H. Kim, Molecular dynamics study of thermodynamic properties of nanoclusters for additive manufacturing, Int. J. Precis. Eng. Manuf.-Green Technol. 4 (2017) 301–306.
[29] F. Rahmani, J. Jeon, S. Jiang, S. Nouranian, Melting and solidification behavior of Cu/Al and Ti/Al bimetallic core/shell nanoparticles during additive manufacturing by molecular dynamics simulation, J. Nanopart. Res. 20 (2018) 133.
[30] A. Brant, M. Sundaram, Molecular dynamics study of direct localized overpotential deposition for nanoscale electrochemical additive manufacturing process, Precis. Eng. 56 (2019) 412–421.
[31] Z. Jiao, C. Song, T. Lin, P. He, Molecular dynamics simulation of the effect of surface roughness and pore on linear friction welding between Ni and Al, Comput. Mater. Sci. 50 (2011) 3385–3389.
[32] Z.S. Pereira, E.Z. Da Silva, Cold welding of gold and silver nanowires: a molecular dynamics study, J. Phys. Chem. C 115 (2011) 22870–22876.
[33] I.S. Konovalenko, I.S. Konovalenko, S.G. Psakhie, Molecular dynamics modeling of bonding two materials by atomic scale friction stir welding, AIP Conf. Proc. 1909 (2017), 020092.
[34] A. Samanta, S. Xiao, N. Shen, J. Li, H. Ding, Atomistic simulation of diffusion bonding of dissimilar materials undergoing ultrasonic welding, Int. J. Adv. Manuf. Technol. 103 (2019) 879–890.
[35] S. Mostafavi, B. Markert, Molecular dynamics simulation of ultrasonic metal welding of aluminum alloys, PAMM 19 (2019), e201900304.
[36] J. Yang, J. Zhang, J. Qiao, Molecular dynamics simulations of atomic diffusion during the Al–Cu ultrasonic welding process, Mater 12 (2019) 2306.
[37] A.R. Riben, S.L. Sherman, W.V. Land, R. Geisler, Microbonds for hybrid microcircuits, Annual Symposium on the Physics of Failure in Electronics (1966) 534–556.
[38] S. Plimpton, Fast Parallel Algorithms for Short-range Molecular Dynamics, No. SAND-91-1144, Sandia National Labs, Albuquerque, USA, 1993.
[39] W. Humphrey, A. Dalke, K. Schulten, VMD: visual molecular dynamics, J. Mol. Graph. 14 (1996) 33–38.
[40] M.S. Daw, M.I. Baskes, Semiempirical, quantum mechanical calculation of hydrogen embrittlement in metals, Phys. Rev. Lett. 50 (1983) 1285–1288.
[41] M.S. Daw, M.I. Baskes, Embedded-atom method: derivation and application to impurities, surfaces, and other defects in metals, Phys. Rev. B 29 (1984) 6443–6453.
[42] K.W. Jacobsen, J.K. Norskov, M.J. Puska, Interatomic interactions in the effective-medium theory, Phys. Rev. B 35 (1987) 7423–7442.
[43] S.M. Foiles, M.I. Baskes, M.S. Daw, Embedded-atom-method functions for the fcc metals Cu, Ag, Au, Ni, Pd, Pt, and their alloys, Phys. Rev. B 33 (1986) 7983–7991.

[44] F.T. Latypov, A.E. Mayer, Shear strength of metals under uniaxial deformation and pure shear, J. Phys. Conf. Ser. 653 (2015), 012041.
[45] S. Murali, N. Srikanth, Y.M. Wong, C.J. Vath, Fundamentals of thermo-sonic copper wire bonding in microelectronics packaging, J. Mater. Sci. 42 (2007) 615–623.
[46] W. Sextro, M. Brökelmann, Intelligente Herstellung Zuverlässiger Kupferbondverbindungen, 8, SpringerVerlag, Berlin/Heidelberg, Germany, 2019.
[47] C. Kaestle, J. Franke, Comparative analysis of the process window of aluminum and copper wire bonding for power electronics applications, International Conference on Electronics Packaging (2014) 335–340.
[48] F.L. Wang, J.H. Li, H. Lei, J. Zhong, Effect of ultrasonic power on wedge bonding strength and interface microstructure, Trans. Nonferrous Met. Soc. China 17 (2007) 606–611.